Ocean Gyre Circulation Changes Associated with the North Atlantic Oscillation*

RUTH G. CURRY AND MICHAEL S. MCCARTNEY

Woods Hole Oceanographic Institution, Woods Hole, Massachusetts

(Manuscript received 7 July 2000, in final form 16 April 2001)

ABSTRACT

Observational evidence is presented for interannual to interdecadal variability in the intensity of the North Atlantic gyre circulation related to the atmospheric North Atlantic Oscillation (NAO) patterns. A two-point baroclinic pressure difference between the subtropical and subpolar gyre centers—an oceanic analogue to the much-used sea level pressure (SLP)-based atmospheric NAO indices—is constructed from time series of potential energy anomaly (PEA) derived from hydrographic measurements in the Labrador Basin and at Station S near Bermuda. Representing the upper 2000-db eastward baroclinic mass transport between the two centers, the transport index indicates a Gulf Stream and North Atlantic Current that gradually weakened during the low NAO period of the 1960s and then intensified in the subsequent 25 years of persistently high NAO to a record peak in the 1990s. The peak-to-peak amplitude difference was 15–20 megatons per second (MT s^{-1}) with a 43-yr mean of about 60 MT s^{-1} a change of 25%–33% occurring between 1970 and 1995. The timing of the ocean fluctuation is organized around the same temporal structure as the NAO index. The two are not directly covariant, but to first order, the ocean signal reflects a time integration, through mixed layer ''memory'' and Rossby wave propagation, of the atmospheric forcing.

To some degree, the gyre PEA histories are fluctuating in antiphase reflecting latitudinal shifts of the surface westerlies across the North Atlantic. Differences in forcing mechanisms and baroclinic responses in each gyre, however, are reflected by divergences in the details of their PEA histories. The subpolar PEA changes are primarily thermally driven through diabatic mixing and surface buoyancy fluxes associated with water mass transformation. Salinity changes, stemming from the occasional passages of low-salinity surface lids (''Great Salinity Anomalies'') through the region, contribute relatively little to the Labrador Basin PEA variability. The interior subtropical gyre PEA history is dominated by quasi-adiabatic vertical displacements of the main pycnocline, and supplemented by changes in the locally formed subtropical mode water as well as by changes in middepth density structure related to advective–diffusive import of Labrador Sea Water.

Multiyear composite fields of North Atlantic potential energy centered in time on the extreme high and low transport periods provide a broad geographic context for the transport index. Basin-scale shifts of oceanic baroclinic pressure gradients between the extreme phases reinforce the sense and amplitude of changes reflected in the Bermuda–Labrador Basin transport index.

1. Introduction

In the past decade, there has been an intensification of efforts toward describing and understanding climate variability in the North Atlantic sector. A significant fraction of that variability is associated with fluctuations in strength and location of the Icelandic low and Azores high atmospheric pressure centers (Rogers 1990). The tendency for sea level pressure (SLP) of these centers to oscillate in antiphase is referred to as the North Atlantic Oscillation (NAO). This NAO seesaw is a perceptible mode of variability throughout the year, but is particularly dominant in winter months (Barnston and Livezey 1987; Rogers 1990). The NAO state may be characterized by an index of that pressure difference (e.g., Hurrell 1995), but the NAO is so strong a mode that alternative indices based on surface air temperature differences (van Loon and Rogers 1978), storms (Rogers 1997), sea ice (Deser et al. 2000), sea surface temperature (SST) patterns (Deser and Blackmon 1993; Kushnir 1994; Sutton and Allen 1997), or SST gradients (Czaja and Marshall 2001), when regressed on SLP, yield much the same dipole SLP anomaly patterns.

When averaged for the winter months, the SLP-based index (e.g., Hurrell 1995) exhibits interannual to decadal and interdecadal fluctuations (Fig. 1). The interpretation of these low frequency fluctuations, including shifts from a quasi-biennial character in the early part of the record to decadal in the later part, are a central part of the ongoing discussion about climate change as we move from the 20th to the 21st century (Hurrell 1996; Hurrell and van Loon 1997; Wunsch 1999). To what degree does the visually prominent fluctuation of the

* Woods Hole Oceanographic Institution Contribution Number 10260.

Corresponding author address: Ruth G. Curry, WHOI, MS #21, Woods Hole, MA 02543.
E-mail: rcurry@whoi.edu

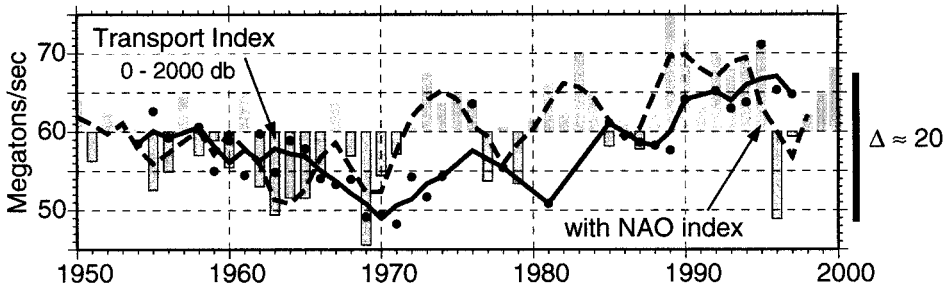

FIG. 1. Baroclinic mass transport index (solid black curve, smoothed with 3-yr running mean) in megatons per second determined from difference in 0–2000 db PEA at the centers of subpolar and subtropical gyres. Black solid circles are unsmoothed annual transport index values. The dashed curve is the SLP-based NAO index of J. W. Hurrell (1995, personal communication) smoothed with a 3-yr running mean. Gray bars represent the annual unsmoothed values of that index (range −5 to 5 with zero centered at the 60 MT s^{-1} line). The net change in transport between extremes is ~20 MT s^{-1}, as indicated on the right axis, with a 50-yr average of ~60 MT s^{-1}.

index over recent decades represent: a global warming response or other nonstationary aspect of the internal fluctuations of the atmosphere, feedback from a slowly evolving ocean, or random fluctuations of a stationary stochastic system?

High and low states of the NAO index reflect enhanced and diminished midlatitude westerlies, with related shifts in wind patterns and intensities of air–sea exchanges of heat (Cayan 1992a,b), freshwater (Hurrell 1996), and momentum (Visbeck et al. 1998). Since the

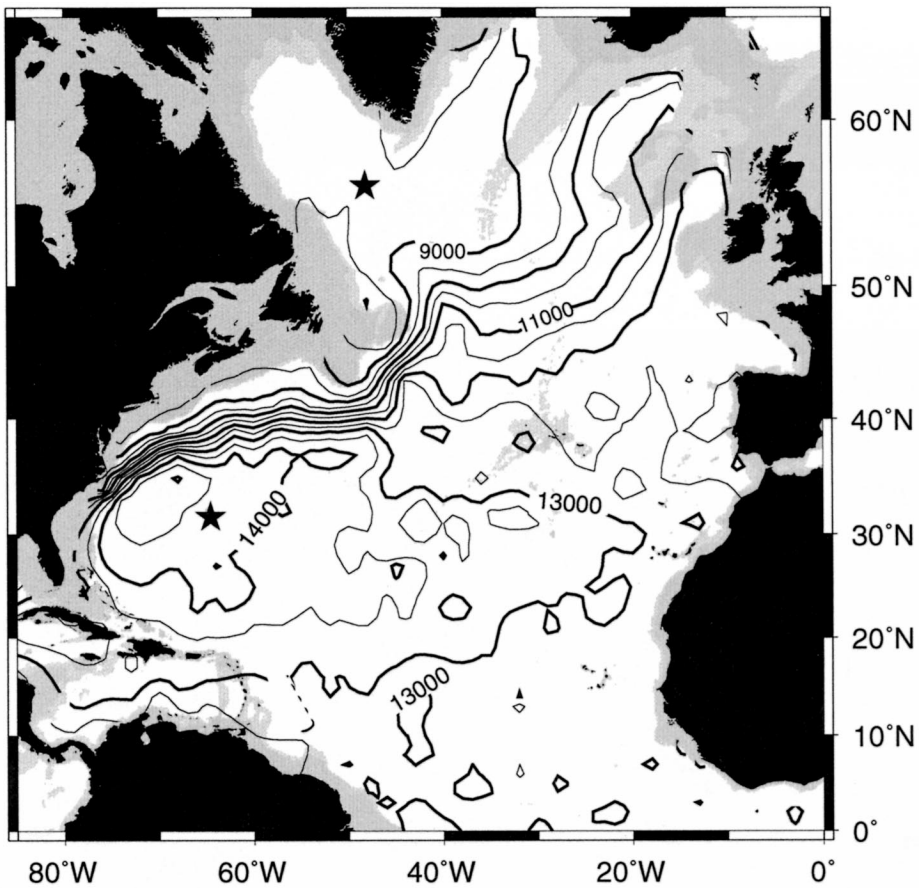

FIG. 2. Climatological mean field of potential energy anomaly (PEA) at the sea surface relative to 2000 db. Contour interval is 500 ergs cm^{-2}. Stars indicate the locations of time series data in the Labrador Basin and near Bermuda used to construct the transport index in Fig. 1.

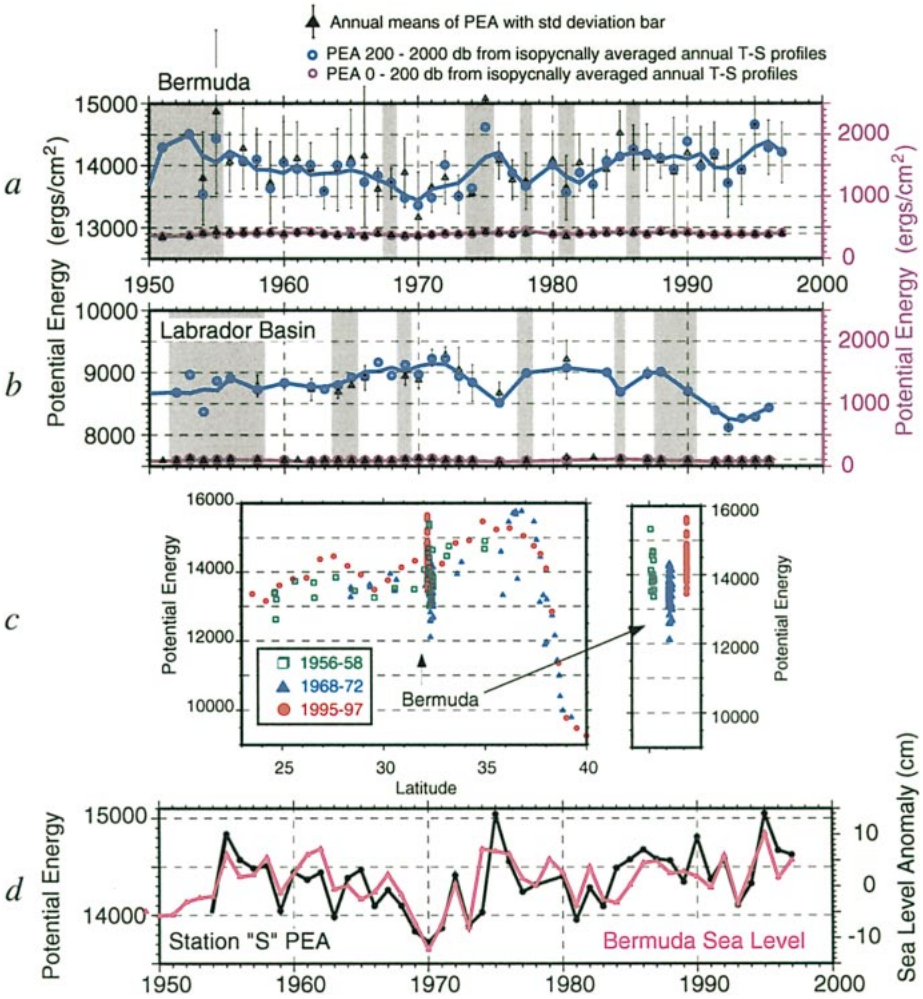

FIG. 3. Time series of PEA at (a) Bermuda and in (b) the Labrador Basin. Blue curves represent annual averages of PEA beneath the seasonally heated layer (200–2000 db, smoothed with a 3-yr running mean; scale is left axis). Purple curves are PEA of the surface layer (0–200 db, scale is right axis). Black triangles represent annual mean PEA derived from individual PEA profiles averaged for each year; vertical bars are standard deviations associated with these annual means. Circles represent PEA values derived from isopycnally averaged annual *T*–*S* profiles. Gray shading indicates years containing less than six measured profiles to compute an annual mean. (c) Latitudinal distribution of PEA from 23° to 40°N comparing individual observations acquired between longitudes 60° and 65°W. Three time frames are differentiated: 1968–72 (blue) corresponding to a shallow thermocline and low subtropical PEA dome, 1995–97 (red) during which the thermocline was deep and subtropical dome high, and 1956–58 (green) corresponding to intermediate dome years. The Bermuda observations are expanded in the panel to the right. (d) Time series of Bermuda mean PEA in ergs cm^{-2} (black curve) and annual mean sea level anomaly (cm) measured by tide gauges at Bermuda (source: Bermuda Biological Station for Research). Both records are annually averaged but unsmoothed values.

general oceanic circulation, including upper ocean gyres and thermohaline overturning, is wind and buoyancy forced, there is little surprise in finding oceanic patterns in the observational record that are coordinated with the low frequency components of atmospheric variability. Notable are SST anomalies that develop directly as a time-integrated response to persistent NAO air–sea heat flux anomalies (Bjerknes 1964; van Loon and Rogers 1978; Deser and Blackmon 1993; Kushnir 1994). The phasing of water mass formation in the subtropical and subpolar gyres and the Nordic Seas is organized around the low frequency atmospheric variability (Dickson et al. 1996; Talley 1996; Lazier 1995). Pioneering work by Levitus (1989a,b) compared pentadal composites of property fields to demonstrate the occurrence of substantial upper ocean heat content anomalies through time. Molinari et al. (1997) sharpened the image of interannual heat content changes in the western subtropical North Atlantic through analyses of XBT measurements. Moreover, multiyear propagation of winter SST

anomalies along the gyre circulation pathways (Hansen and Bezdek 1996; Sutton and Allen 1997; Mazoguchi et al. 1999) suggests that variability of oceanic heat content embodies more than just a stationary, passive response to the atmosphere. There is evidence also of interannual propagation in the SLP distributions themselves (Halliwell 1997).

If the NAO SLP–SST–heat content fluctuations were the only signals of coordinated atmosphere–ocean variability, then that association would be amenable to a null hypothesis explanation: that the ocean integrates atmospheric forcing to redden the spectral response relative to the forcing spectrum (Hasselmann 1976; Frankignoul and Hasselmann 1977). Battisti et al. (1995), for example, hindcast winter SST for the North Atlantic using observed atmospheric circulation anomalies and an ocean simulated as a field of one-dimensional mixed layers atop a diffusive deep ocean (no advection). The relative success of this and similar SST hindcasts for large areas of the North Atlantic has given considerable weight to the idea of mixed layer integration of surface heat flux as the leading mode of extratropical ocean–atmosphere interactions. However, this simulation included an artificially prescribed climatological annual mean and seasonal cycle of convergence of heat by the ocean, since the omission of oceanic advection precludes such convergence. This particular example of a simple hindcast model failed in the regions corresponding to the strong advection regimes of the Gulf Stream—the site of maximum observed oceanic convergence of heat. It suggests that anomalies of ocean heat advection and convergence play a role in setting SST in at least that area. Such anomalies could result from advection of heat content anomalies by the mean oceanic circulation or by an oceanic circulation that itself is anomalous.

The upper ocean's mean advective–diffusive heat balance involves a large annual surface heat flux from the midlatitude ocean into the overlying atmosphere, supported by oceanic heat transport convergence into the region. Thus SST anomalies are more than merely one-dimensional mixed layer responses to local atmospheric forcing; they reflect departures of the heat balance from the climatological annual mean and seasonal cycles. These departures can lead to interannual persistence of winter SST anomalies through a reemergence mechanism (Alexander and Deser 1995) whereby a winter mixed layer anomaly is seasonally sequestered beneath a summer thermocline and then reappears in the subsequent winter. The observations indicate that this mechanism acts both locally (viewing as an Eulerian field) and in a Lagrangian framework. Underlying the decadal evolution of the observed oceanic heat content patterns are not only the thermal inertia of winter mixed layer dynamics but also modulations of the ocean gyre circulation. Several studies have employed ocean circulation models with prescribed forcing variability (estimated from observations) to investigate aspects of oceanic heat content and circulation variabilities (e.g., Sturges and Hong 1995; Halliwell 1998; Sturges et al. 1998; Häkkinen 1999, 2000; Ezer 1999). More process-oriented modeling efforts have also addressed the issue of coordinated participation of the ocean and atmosphere in climate variability, both coupled and uncoupled (e.g., Delworth et al. 1993; Delworth 1996; Capotondi and Holland 1997; Saravanan and McWilliams 1997, 1998; Frankignoul et al. 1997; Griffies and Bryan 1997; Visbeck et al. 1998; Grötzner et al. 1998; Saravanan et al. 2000). The interpretations of such models explore the dynamics of low frequency fluctuations of the ocean. What information regarding interannual ocean variability can the observational record provide with respect to these studies?

The present paper examines observational evidence for interannual to interdecadal variability of the circulation intensities of the North Atlantic subtropical and subpolar gyres. Hints of such circulation variability were evident in the pentadal comparisons by Levitus (1990), Greatbatch et al. (1991), and Greatbatch and Xu (1993). We can improve on those beginnings with ~15 years additional hydrographic data spanning an extreme NAO episode in this most recent decade. We focus in particular on two sites with extended time series of data and use them to construct an oceanic analogue of the atmospheric NAO index: a two-point baroclinic pressure difference between the subtropical and subpolar gyre centers. This can be scaled so as to represent the eastward transport along the gyre–gyre boundary—the ocean's ''westerlies''—completing the analogy to the atmosphere index. As shown in Fig. 1, this transport index exhibits a range of ±17% through its span of 43 years, a substantial variability that visually is decadal in character. The transport time series indicates a gyre circulation that gradually weakened during the low NAO period of the 1960s and then intensified in the subsequent 25 years of persistently high NAO to a record peak in the 1990s.

In section 2, we discuss the basis for and general character of the oceanic transport index of Fig. 1. Section 3 describes the data used for the index, how the transport index relates to the individual subpolar and subtropical gyre histories, and its dependence on changes in deep density structure as well as thermocline variability. Section 4 examines the character of the two indices of Fig. 1, focusing on the possibility that the oceanic index reflects a weighted time integral of the NAO index. Section 5 describes basin scale shifts of oceanic baroclinic pressure gradients by contrasting multiyear composite fields centered in time on the extreme high and low transport periods. Section 6 provides a summary and some concluding remarks.

2. An oceanic NAO index

Expressed as anomalies of SLP, the NAO atmospheric seesaw is a dipole with subtropical and subpolar centers

located southwest of Iceland and over the Azores. Seeking to maximize time resolution and length of the available record, SLP measurements from a pair of observation sites near those action centers have come into use as the basis for an NAO index. Hurrell (1996) uses sites in Iceland and Portugal for a much-illustrated wintertime (DJFM) NAO index (Fig. 1) that extends backward to 1865. Jones et al. (1997) similarly used sites in Iceland and Gibraltar to extend the record to 1823. The SLP difference between these locations provides an indication of changing atmospheric mass distributions that are associated, through the thermal wind relation, with changes of strength and geography of the surface westerlies from northern North America across the Atlantic into northern Eurasia. Although such two-point indices may be less than optimal for capturing the basin-scale NAO (e.g., Deser 2000), they continue to be used because of the homogeneity of their data, high sampling frequency, and long duration, much longer than the period for which reliable SLP fields are available for spatial EOF analysis.

An oceanic analogue to these SLP patterns is manifested in the North Atlantic dynamic height and potential energy anomaly (PEA) distributions, which provide information regarding the magnitude and geography of geostrophic velocities and mass transports. The climatologic mean PEA field is depicted in Fig. 2 for the sea surface relative to 2000 db for which PEA, χ, is (see Fofonoff 1962) the vertical integral of the specific volume anomaly, δ, multiplied by pressure, p, and with δ and p calculated using algorithms developed by Fofonoff and Millard (1983):

$$\chi = \frac{1}{g}\int_{p=2000}^{0} p\delta \, dp.$$

PEA is related to dynamic height, DH $= \int \delta \, dp$, effectively weighted by p/g, and has units of ergs cm^{-2}. PEA is a depth-averaged property reflecting the density stratification and heat content of the ocean well below the wind-driven layer, not just conditions at the sea surface. The terms χ and DH approximate stream functions for the baroclinic mass transport fT_m and baroclinic horizontal velocity fu, respectively, where f is the Coriolis parameter.

The contours of Fig. 2 indicate that the horizontal gradient of PEA is concentrated in the Gulf Stream–North Atlantic Current system, while the interiors of the two gyres are relatively homogeneous. Bermuda and the central Labrador Basin, located near the center of each gyre and for which exist relatively long instrumental records, are thus representative of general conditions in the gyre interiors. These high and low PEA centers of the subtropical and subpolar gyres, respectively, are analogous to the Azores high and Iceland low SLP centers which embody the atmospheric NAO index and delimit the strength of the westerly winds. For the ocean, the difference of PEA at the centers of these two gyres, χ_B and χ_{Lab}, divided by an appropriate Coriolis parameter f, provides an index of the baroclinic mass transport and, hence, the strength of the eastward baroclinic flow along the boundary between the gyres:

$$T_m = \frac{\chi_B - \chi_{Lab}}{f}.$$

The units of T_m are megatons per second (MT s^{-1}), where 1 MT s^{-1} is within a few percent of the volumetric unit of transport (Sv $\equiv 10^6$ m^3 s^{-1}). For the climatologic mean, PEA (0–2000 db) near Bermuda is ~14 300 ergs cm^{-2} and ~8700 ergs cm^{-2} in the Labrador Basin yielding an average transport of approximately 60 MT s^{-1} using f corresponding to 40°N, the average latitude of the concentrated PEA gradient. The index that results from the time histories at these two locations is shown in Fig. 1. We shall shortly discuss the representativeness of these two specific locations as indicators of basin-scale changes in vertical density structure and thus of the baroclinic gyre circulation.

As with geostrophic velocity, this transport index represents relative, not absolute, quantities, for it assumes negligible tilt of isobars at some reference level. A deep reference level is appropriate for such geostrophic calculations for the Gulf Stream and North Atlantic Current. The unidirectional shear from top to bottom in these flow regimes is thought to convert to eastward flow throughout the water column (Fuglister 1963; Worthington 1976; Clarke et al. 1980; Meinen et al. 2000; Sy 1988; Sy et al. 1992). We emphasize, however, that the resulting transport index pertains only to the baroclinic components of the flow. Thus, unlike the direct relation between SLP gradient and the surface geostrophic winds, the oceanic transport index denotes the relative geostrophic flow along the gyre–gyre boundary, which, as Fig. 2 indicates, is concentrated in the Gulf Stream–North Atlantic Current system.

The transport index is compared with Hurrell's atmospheric NAO index in Fig. 1; both raw annual values and 3-yr running means are given for each. The transport index displays an organized progression from high to low in the 1950s and 1960s, a brief rise and fall in the 1970s, followed by a sustained increase in strength throughout the 1980s to maximum values in the 1990s. The amplitude of change from its minimum circa 1970 to its maximum in the mid-1990s is 15–20 MT s^{-1}; for a mean transport of approximately 60 MT s^{-1}, this change amounts to a range of about 25%–33% over 25 years.

The average transport of 60 MT s^{-1} for the climatological mean PEA difference between Bermuda and the Labrador Basin is similar to the magnitude of transport expected from flat-bottomed Sverdrup dynamics calculations; for example, the geostrophic transports estimated by Leetmaa and Bunker (1978; hereafter LB) from wind stress distributions compiled by Bunker (1976). Their maps (LB Fig. 4) indicate a subtropical anticyclonic geo-

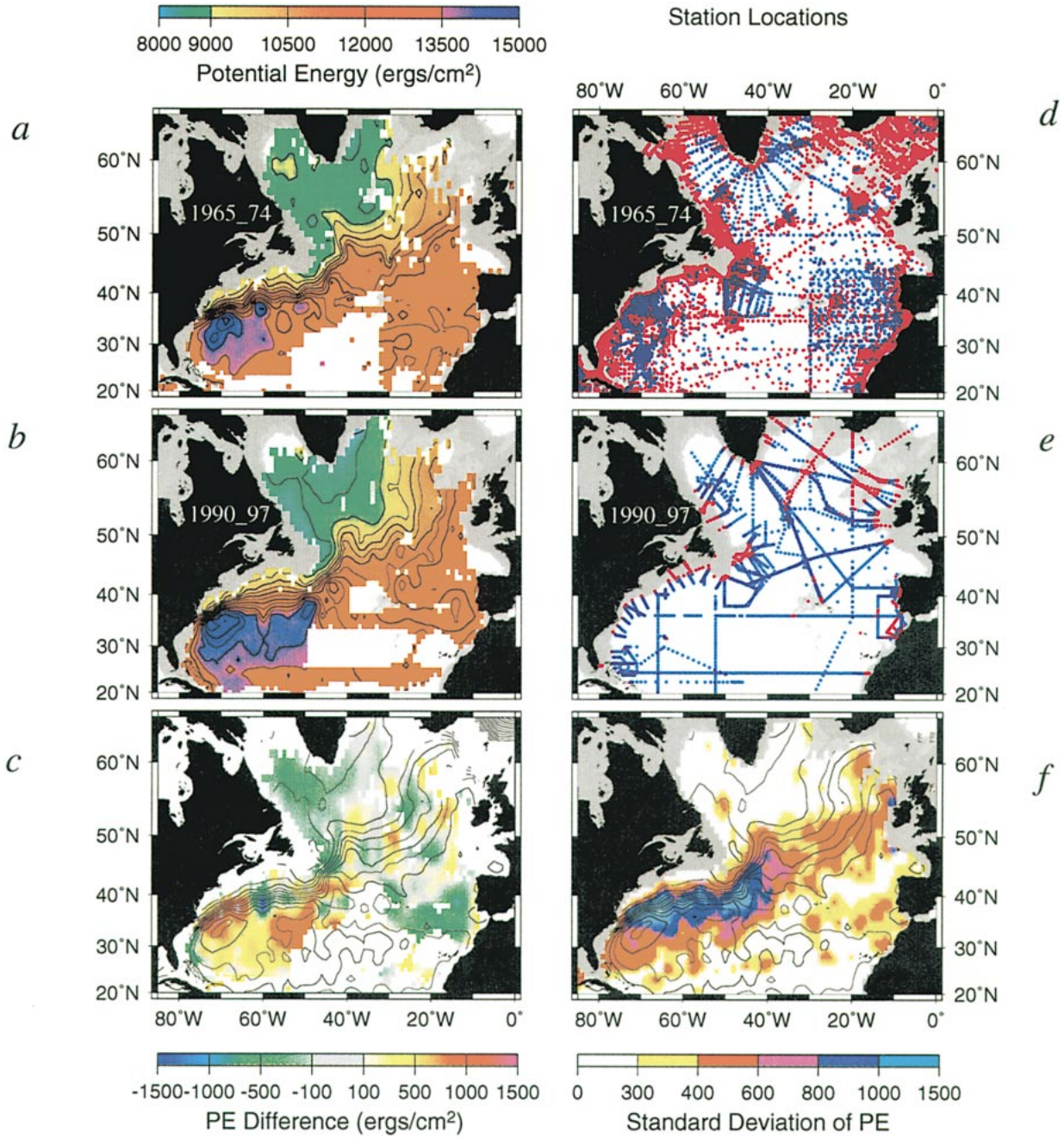

FIG. 4. PEA 200–2000 db distribution for the time frame spanning (a) the low transport index years 1965–74. and (b) the high transport years 1990–97. Gray shading depicts bathymetry <2000 m. White areas indicate no observations made within 2° lat–long radius. (c) Difference of PEA distributions between extreme transport years (a − b) is depicted with color (yellow–red colors indicate increased PEA in the later time frame, green–blue colors indicate diminished PEA, gray shading indicates neglible change). Contours are the climatological mean PEA distribution from Fig. 2. White areas indicate that no difference could be computed due to a lack of data in one or both time frames. (d) Location of measured profiles available for the low transport years, 1965–74, from which the field in (a) was constructed. Red dots indicate that measurements did not reach to 2000 m; blue dots represent profiles exceeded 2000-m depth. (e) Same as (d) but for the high transport years, 1990–97, from which the field in (b) was constructed. (f) Standard deviation of climatological PEA distribution computed at 1° grid intervals. Contours depict the climatological mean PEA distribution as in (c).

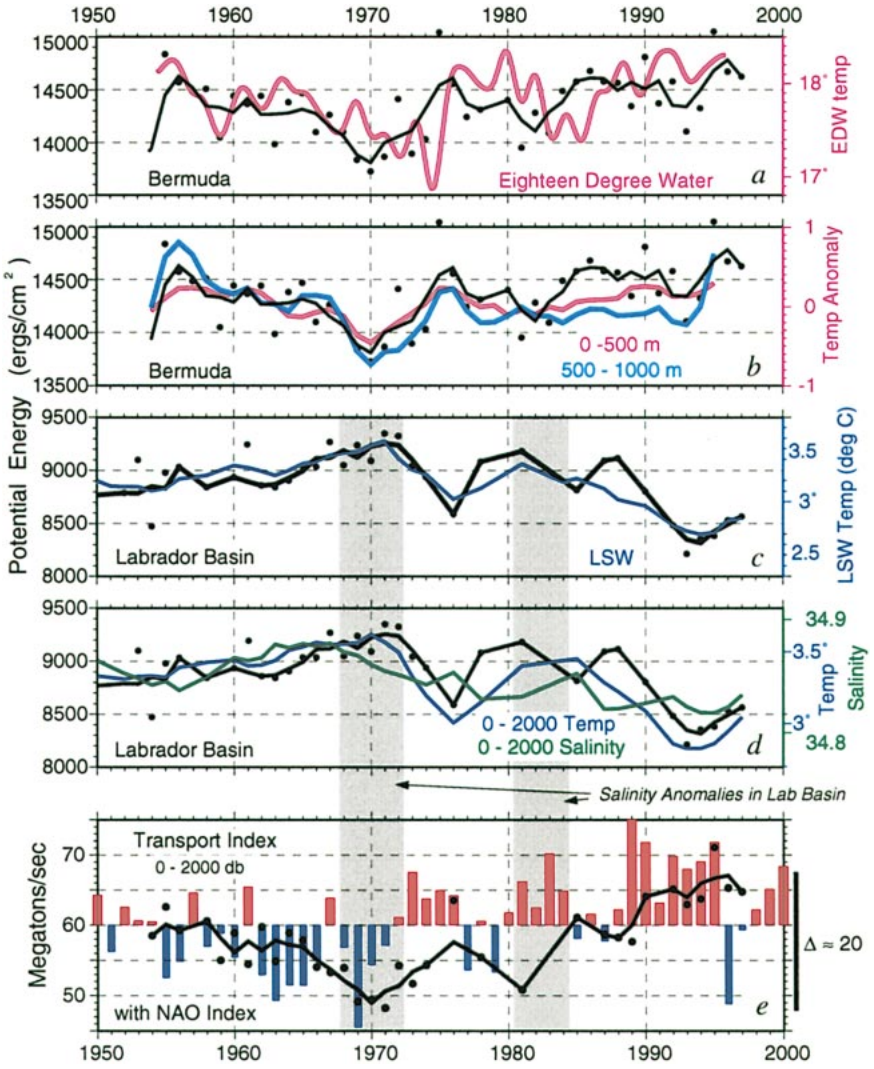

FIG. 5. Time series of PEA at (a and b) Bermuda (black circles are annual averages, black curves are 3-yr running means, left axes give scales). (a) EDW temperature (magenta curve and right axis) from Talley (1996); (b) temperature anomaly in two thermocline layers 0–500 m (magenta) and 500–1000 m (blue) from an analysis by Joyce and Robbins (1996). (c and d) Time series of PEA, as above, but from the central Labrador Basin with scale given by the left axes. (c) The time series of LSW core temperature (at 1500 db) with the blue curve and right axis; (d) The vertically averaged (0–2000) temperature and salinity by the blue and green curves, respectively, scales are labeled on the right axis. Yellow shaded bars indicate periods when low salinity surface lids occupied the Labrador Basin. (e) Transport index (as in Fig. 1) that is derived from the difference of PEA at the two above locations. Pink and blue bars are the SLP-based NAO index (Hurrell 1995).

strophic flow of 30–35 MT s^{-1} and a subpolar cyclonic gyre of 25–30 MT s^{-1}, the combined signal totaling 55–65 MT s^{-1}. Cyclonic wind forcing of the slope water produces geostrophic transports of 10–15 MT s^{-1} in LB and thus an estimate of about 45 MT s^{-1} for the Gulf Stream flow between the subtropical gyre and slope water gyre. The PEA difference between the slope water and Bermuda indicates a mean transport of about 50 MT s^{-1} (Fig. 2). Because the Bunker wind stress data spanned the years 1941–72, it would have been influenced by the predominantly low NAO wind patterns of that period and thus potentially produced lower transports than those that would have resulted if the 25 years of subsequently high NAO conditions had been incorporated (as in the ''mean'' PEA map of Fig. 2).

Although our transport index somewhat echoes the trends of the atmospheric index—the gyre circulation weakening during persistently low NAO index and strengthening during high NAO index (Fig. 1)—these indices are not directly covariant. The cross-covariance of the unsmoothed time series (for which gaps in the oceanic index were interpolated with a cubic spline) is

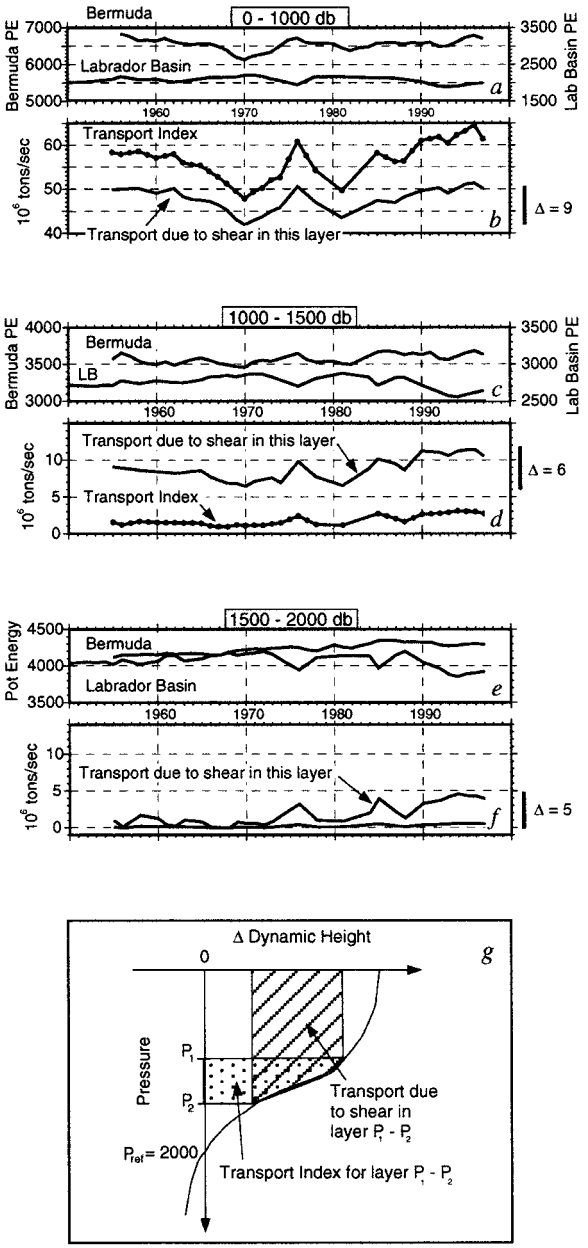

FIG. 6. Time series of (a) the upper layer (0–1000 db) PEA at Bermuda (top curve, left axis) and in the Labrador Basin (bottom curve, right axis). (b) Transport index for the mass transport in the 0–1000 db layer and for the amount of 0–2000 total transport attributed to the geostrophic shear in this layer. The net transport change incurred due to changes of shear in the layer, $\Delta = 9$ MT s^{-1}, is annotated by the right axis. (c and d) As in (a and b) but for the layer 1000–1500 db. The 0–2000-db total transport that accumulates on account of shear in this layer is greater than the amount transported in this layer. The change in total 0–2000 transport due to shear is about 6 MT s^{-1}. (e and f) As in (a and b) but for the deep layer 1500–2000 db. Changes of shear in this layer contribute an additional 5 MT s^{-1} to the total 0–2000 db in the latter portion of the record. (g) Profile of dynamic height difference ($\propto$ geostrophic shear) whose vertical integral yields transport. This schematic distinguishes between transport in a layer P_2–P_1 (dotted area) vs total 0–2000 transport due to shear in a layer (hatched area).

characterized by a correlation coefficient $r = 0.32$ (significant at the 95% level in the Student's t-test for 27 or more degrees of freedom) which improves somewhat at lags of 1–2 yr with $r = 0.58$ (95% significant for 10 or more degrees of freedom). Indeed, the peaks and valleys of the two smoothed time series post-1970 (Fig. 1) give some indication that the oceanic index lags behind the atmospheric index by perhaps a year or two. A simple lag, however, falls short of producing a strongly covarying relationship between the two indices, especially prior to 1970. We will elaborate on this point in a later section.

In the remainder of this paper, we focus on the physical processes that contribute to the fluctuation of the oceanic circulation index, recognizing that, although we may find ocean signals that track the NAO index in interesting ways, correlation does not necessarily establish causality—especially given the brevity and spatial sparsity of the oceanic record. For the upper 2000 db at these two locations, two general types of ocean responses to NAO forcing are differentiated: one essentially local and winter mixed layer in nature (e.g., water mass transformation involving heat flux and wind stress anomalies), the other more dynamical and involving the ocean's internal baroclinic adjustment (e.g., long Rossby wave induced vertical thermocline displacements, intergyre movement of upper ocean anomalies, and mid-depth movement of potential vorticity anomalies). Although interactions between barotropic forcing of the circulation and topography can also result in a baroclinic response (e.g., as in Greatbatch et al. 1991), we do not expect that topographic influences play an important role in the 0–2000 db baroclinic variability of these interior gyre locations. Because these primary modes of oceanic response alter the vertical density structure of each gyre, they lead to a secondary mode of response: strengthening or weakening of the baroclinic basin-scale horizontal and overturning circulations. The timescales of these processes, together with the observed low frequency fluctuation of the atmospheric NAO forcing, are likely to be fundamental in setting the pace and amplitude of the oceanic response.

3. Data and analysis

a. Data sources and the variability of potential energy

The hydrographic profiles used for the transport index were obtained from and analyzed with HydroBase (Lozier et al. 1995; Curry 1996). These include 998 (near Bermuda) and 376 (Labrador Basin) bottle and CTD pressure, temperature, and salinity profiles spanning the years 1950–97; their location is shown in Fig. 2. Figures 3a,b display annual means and standard deviations of PEA at each of the gyre centers and contrasts the seasonally heated layer (upper 200 m) with the remaining water column (200 db relative to 2000 db).

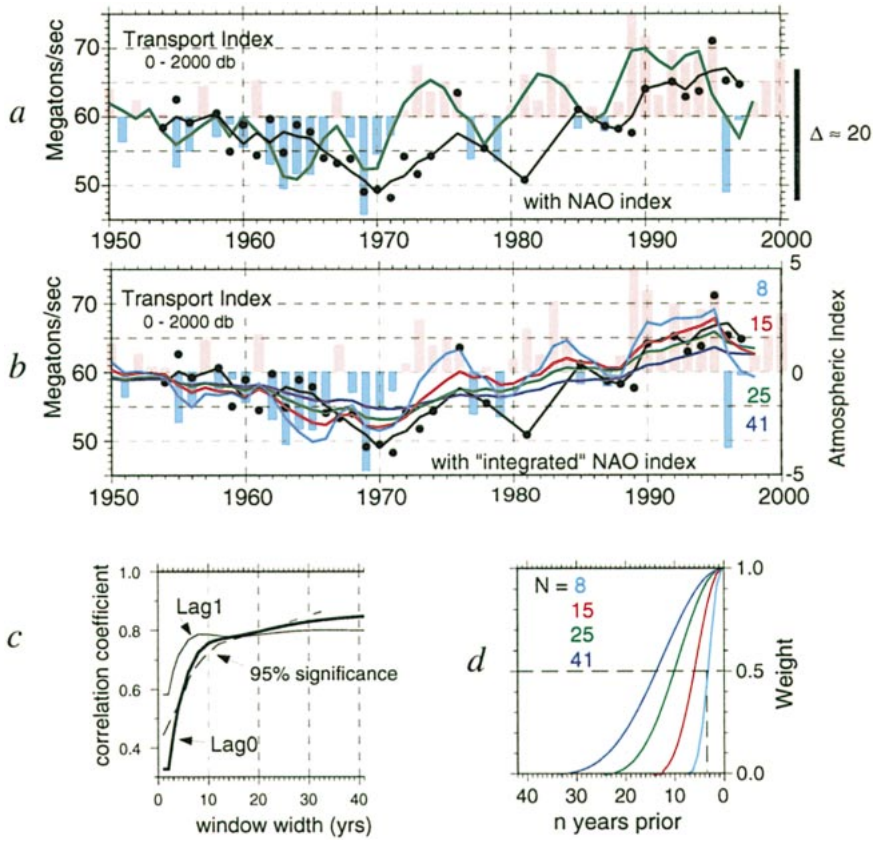

FIG. 7. (a) Transport index (black curve) with atmospheric NAO index (Hurrell). Pink and blue bars are the annual NAO index values, the green curve is the index smoothed with a 3-yr running mean. The time series ranges from 1950 to 1998. (b) Transport index as in (a). Colored curves represent NAO index filtered with a one-sided Blackman window to simulate ocean ''memory.'' The colors depict various window widths (8, 15, 25, and 41), which are annotated near the right axis. (c) Correlation of transport index and the ''integrated'' NAO index as a function of filter window width. Heavy black curve is the lag-0 correlation, thin black line is the lag-1 correlation, and the dashed line shows the 95% confidence limits determined from the effective degrees of freedom (length of the oceanic record divided by the integral timescale). (d) Shape of the weighting function implemented in the Blackman filter for various window widths (N). The horizontal dashed lines indicates the half-weight line (for reference only) to demonstrate that most of the weight, or ''memory,'' is concentrated in the portion of the window spanning from 0 to 0.4 N.

Results from two methods of deriving annual PEA values are shown: 1) summing individual PEA determined from each measured profile to obtain a mean annual value (black triangles) and 2) isopycnally averaging all potential temperature–salinity (θ–S) profiles within a year and computing PEA from the resulting annual mean temperature and salinity profiles (colored circles). The former method provides information concerning the intra-annual variability of potential energy, which is lost in the latter method. However, because a significant number of individual profiles are not vertically continuous enough from 0 to 2000 db to yield reliable potential energy information, especially true for bottle casts, method 1 produces annual means that are more vulnerable to aliasing through the loss of information. Isopycnally averaging the individual θ–S profiles provides a sensible estimate of annual PEA values using all available measurements without requiring each individual profile to be vertically continuous. The isopycnally averaged values of the subtropical time series are thus less erratic than the mean of the individual potential energy profiles (Fig. 3).

The seasonal cycle, whose effects are largely restricted to the upper 200–300 m, represents a small amount of the total (0–2000 db) intraannual variance [10%–20% according to Sato and Rossby 1995]. Potential energy and intraannual standard deviations for the upper 200 db layer have been plotted (purple curves, Fig. 3) at the same scale as the full 200–2000 db values to illustrate that this seasonal layer has relatively small impact on the interannual variability of the 0–2000 db layer. This arises in part from the weighting by p/g in the PEA formulation and the vertical integration of structural changes at depth. Standard deviations in the seasonally

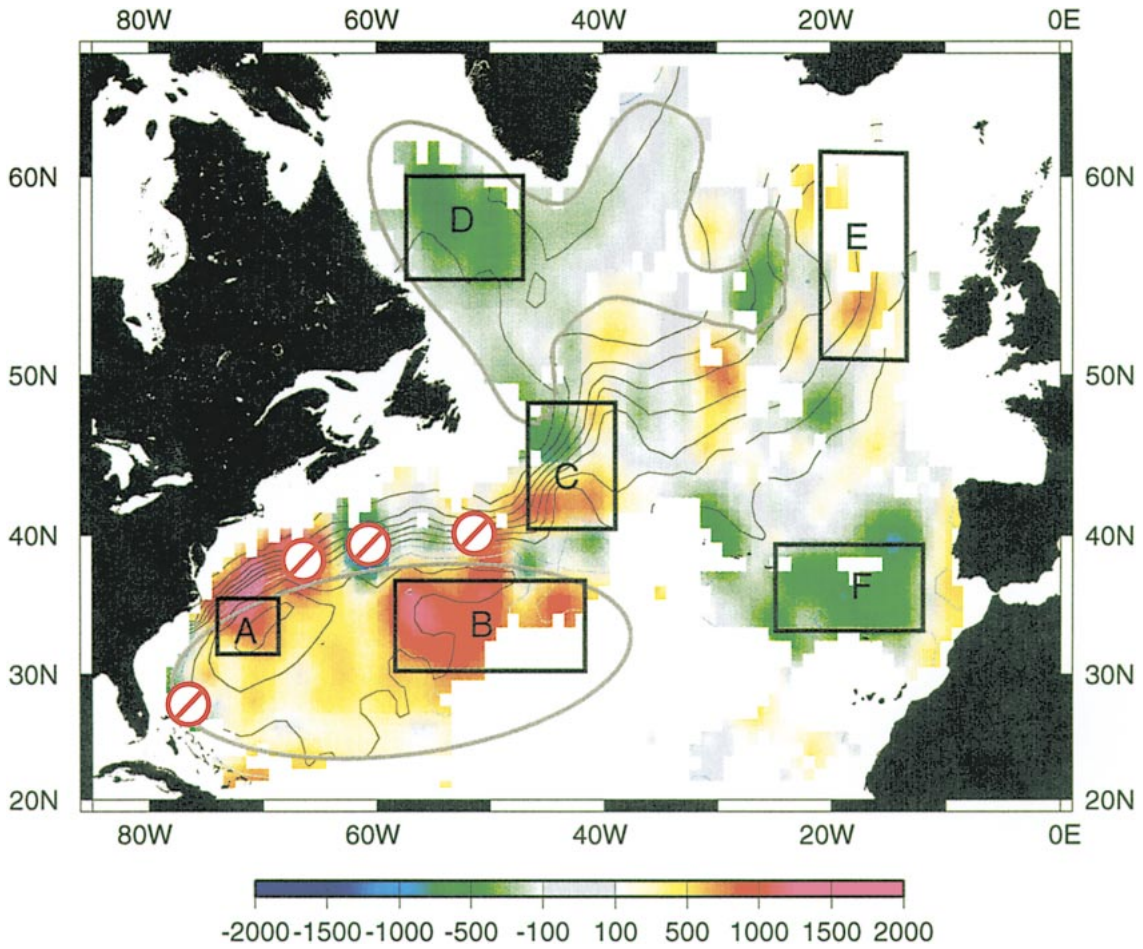

FIG. 8. Difference of PEA distributions between extreme transport years, enlarged from Fig. 4c. The regions corresponding to the western basin interior gyre dipole are outlined. Six areas of large differences to which the text refers are labeled by boxes **A**–**F**. The white circles with a red diagonal slash mask areas of the Gulf Stream where high gradients and sparse data introduce misleading ''signals.'' PEA difference is depicted with color: yellow–red colors indicate increased PEA in the high transport time frame, green–blue colors indicate diminished PEA, gray shading indicates neglible change. Contours are the climatological mean PEA distribution from Fig. 2. White areas indicate no difference could be computed due to a lack of data in one or both time frames.

heated layer are typically 5%–10% of the annual mean values: 20–30 ergs cm^{-2} in the subtropics and 5–10 ergs cm^{-2} in the subpolar regions. Interannual variances in this layer are also quite small: annual mean potential energy of the upper 200 db ranges 400 $\pm$ 30 ergs cm^{-2} in the subtropics and 100 $\pm$ 15 ergs cm^{-2} in the Labrador Basin.

Below the seasonally heated layer, the two sites show markedly different intraannual variability. In the central Labrador Basin, intraannual variability of PEA is small relative to its low frequency interannual signal. The average intraannual standard deviation, or rms, is approximately 120 ergs cm^{-2} compared to $\sim$1000 ergs cm^{-2} change over 20 years. Post-1980, the rms decreases to about 80 ergs cm^{-2} presumably due to technological improvements including the increased availability of high-resolution CTD profiles. This small variance is not merely the result of sparse sampling in this region but instead reflects the small impact that regional eddies exert on the Labrador Basin potential energy field. In contrast, the subtropics show a similar long-term change of $\sim$1000 ergs cm^{-2} but the rms is approximately 480 ergs cm^{-2}, reflecting a much greater influence of eddy activity.

The Bermuda PEA signal appears to reflect a combination of the variable intensity of the basin-scale subtropical gyre ''dome'' (elevated sea surface relative to geoid) and a mesoscale eddy field transiting the region (smaller-scale domes and depressions). Alterations of the western subtropical dynamic height field have been shown to occur on basinwide geographic scales and at decadal time scales (Levitus 1990; Greatbatch et al. 1991). Comparing PEA at the extremes of the subtropical signal strongly suggests that the general structure of the gyre changed little but that the entire western subtropical dome was either higher or lower at these times. In Figs. 4a and 4b (which will be discussed later in more detail) PEA fields composited for the time pe-

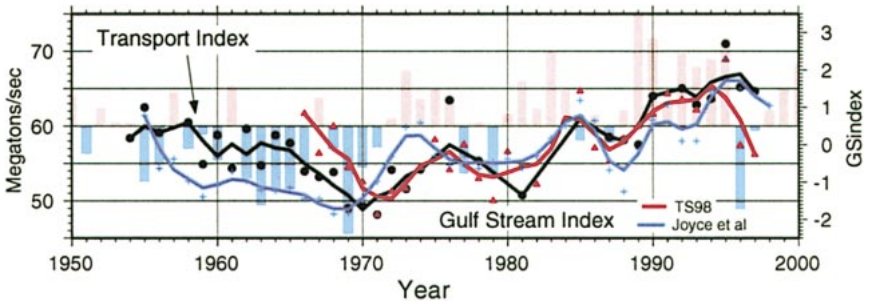

FIG. 9. Covariance of transport index (black curve and circles) with two versions of a Gulf Stream index, which reflects latitudinal shifts of the mean Gulf Stream position west of 65°W. Taylor and Stephens (1998) index is the red curve and triangles; the cyan curve and crosses is a version as in Joyce et al. (2000) but restricted to the region of the Gulf Stream west of 65°W. Correlation coefficients are $r = 0.74$ for Taylor and Stephens and $r = 0.69$ for Joyce et al.

riods 1965–74 (subtropical dome low) and 1990–97 (dome high) show that changes occur over the entire western basin. An examination (Fig. 3c) of PEA values from 60°–65°W versus latitude for three distinct time periods—1995–97 (high dome), 1956–58 (intermediate dome), 1968–72 (shallow dome)—supports the image of a gyre-scale raised or lowered thermocline. The rms of individual Bermuda Station ''S'' PEA values, clustered near 32°N, is approximately the same (~500 ergs cm^{-2}) within each of the three time periods, but the range of values for the years 1995–97 (13 400–15 500 ergs cm^{-2}) and 1968–72 (12 100–14 300 ergs cm^{-2}) are distinctly offset relative to one another. The intermediate dome years, 1956–58, possess a similar variance but a range intermediate between the two extremes (13 000–15 000 ergs cm^{-2}). The latitudinal distribution of PEA, gently increasing northward to the Gulf Stream where it then falls off rapidly, is consistent among the three time periods indicating a rather stable gyre geometry: that is, the Bermuda signal is not indicative of the gyre center migrating back and forth across that location but instead an expanding or contracting gyre dome. The variance derives from a substantial eddy field passing through this location. Since most of these eddies are cyclonic in nature, their influence will, if anything, bias the mean PEA somewhat lower, not higher, and will thus tend to underestimate, not inflate, the transport index values.

Consistent bimonthly sampling throughout the year at Station S seems to adequately resolve the low frequency variability despite the vigorous mesoscale. The most compelling evidence comes from a very close parallel between the PEA signal and the sea level record independently measured by tide gauges at Bermuda (illustrated in Fig. 3d), the tide data having high temporal resolution required to resolve the diurnal cycle. Covariance of the unsmoothed annual mean values is significant (>99%) with a correlation coefficient of 0.75 for the years 1954–97. Thus, while we do not have an oversampled hydrographic time series to directly demonstrate the adequacy of bimonthly sampling, the high resolution tidal record serves as a proxy and suggests that bimonthly hydrography is adequate for recognizing the interannual signals without excessive aliasing by mesoscale variability. Moreover, this strong correlation affirms the conclusion by Frankignoul et al. (1997) that low vertical mode baroclinic signals dominate the barotropic signals at low frequencies and suggests, by inference, a baroclinic dominance of subtropical sea level changes.

Comparing Figs. 3a and 3b, the low frequency signals of the two gyres appear to be approximately out of phase with one another. This is brought out more clearly by application of a three-point running mean (Figs. 3a and 3b, blue curves) to the annual averages, which educes low frequency organization in both subtropical and subpolar regions mirroring one another. As with the atmospheric NAO phenomenon, the oceanic time series are indicating a seesaw mode of variability. Because the oceanic data describe primarily a single multidecade cycle of the seesaw, with one or two lower amplitude fluctuations of shorter duration, the seesaw is a tentative characterization, subject to future monitoring of oceanic signals and to sorting out how the ocean dynamics might lead to this mode of fluctuation.

In addition to the opposite phasing of the two signals, the oceanic seesaw involves a surprising amplitude symmetry. The individual time series of 0–2000 db PEA at the gyre centers, Fig. 5, indicate that the peak-to-peak magnitude of the transport change derives equally from changes of vertical density structure in both the subpolar and subtropical regions. That is, the 0–2000 db transport change over 25 years is ~20 MT s^{-1} yet only 10 MT s^{-1} is attributable to the subtropical PEA history. As there is little a priori reason to suggest that these should be numerically the same amplitude, this result is rather intriguing. It hints at a dipole character to the subpolar–subtropical ocean signals that reaches deeper than just its SST manifestation (e.g., Deser and Blackmon 1993; Kushnir 1994) and further underscores the analogy between the oceanic transport fluctuation and the NAO phenomenon.

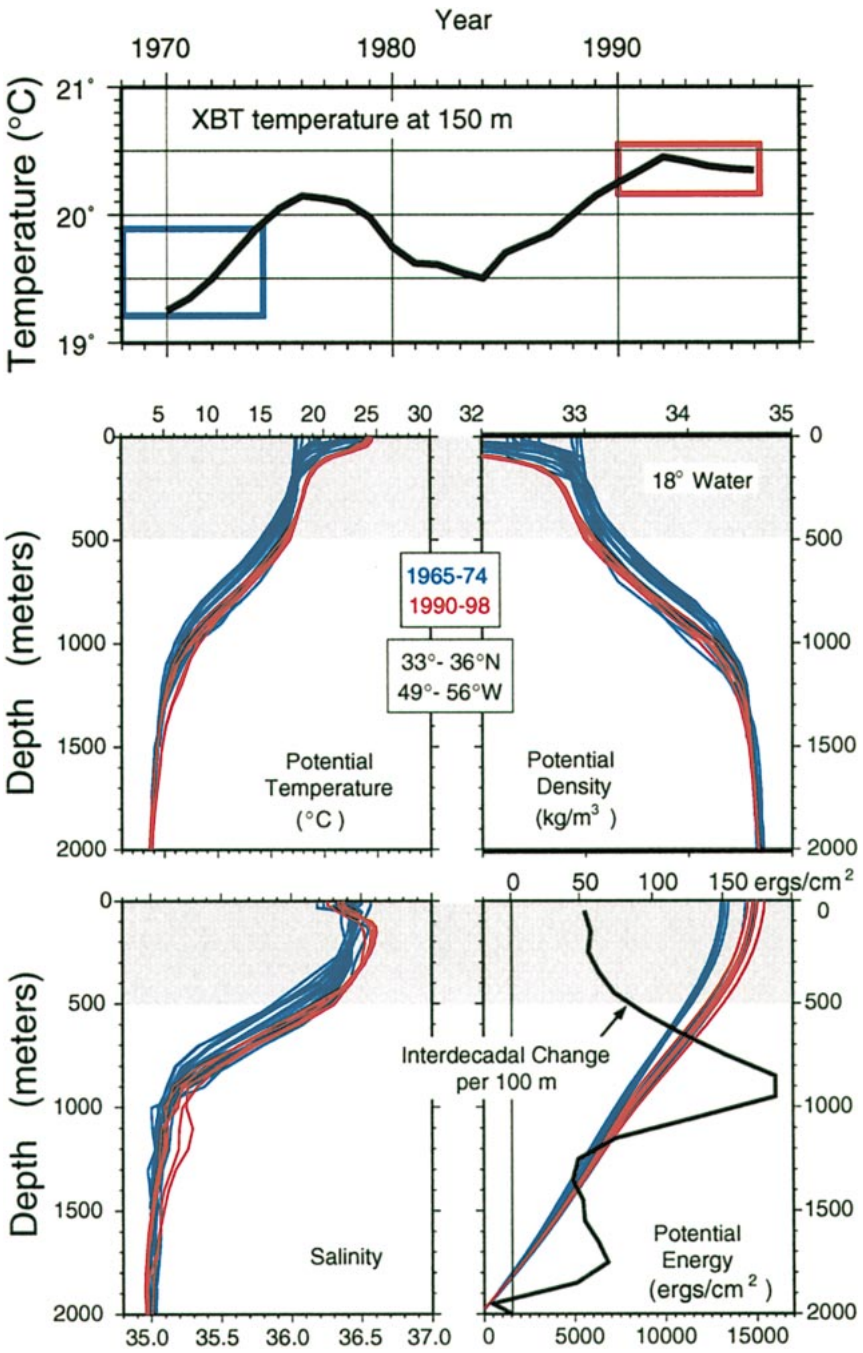

FIG. 10. Observed properties from the EDW formation region, labeled box **B** in Fig. 8. The top panel is a time series of temperature at 150 m from XBT measurements in the geographic area 34°–37°N, 50°–54°W (as in Molinari et al. 1997, but updated for this region by R. Molinari 2000, personal communication) Red and blue boxes mark the years of high and low transport extremes. The remaining panels are vertical profiles of potential temperature, density, salinity, and potential energy in the area 33°–36°N, 49°–56°W (the EDW formation region labeled box **B** in Fig. 8) at the extreme phases of the transport index: 1965–74 (blue curves) and 1990–98 (red curves). The curves represent the isopycnally averaged profiles in each 1° grid square within that geographic area for each time period. No additional smoothing has been performed. The gray shaded band in each panel depicts the depth range of the EDW. The black curve in the lower right panel (PEA profiles) reflects the magnitude of change between the two time periods for each 100-m depth increment; the scale is on top axis.

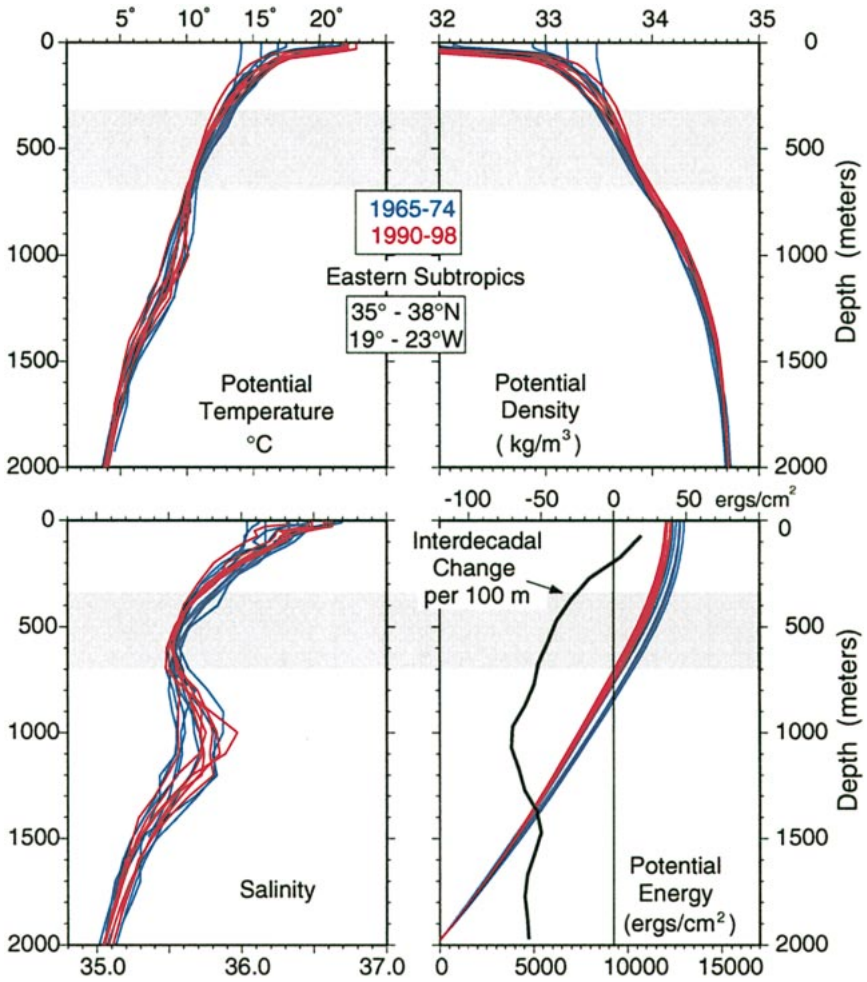

FIG. 11. Same as Fig. 10 but for the box labeled **F** in Fig. 8. Blue curves reflect low transport index years, red curves are high transport index years. Gray shading gives the depth range of the main thermocline. The black curve in the lower right panel is the PEA change between time frames per 100-m interval; its scale is on the top axis of that panel.

This dipole behavior is less than statistically robust, however, because those statistics are limited by the length of instrumental records and affected by gaps in the subpolar time series, particularly between 1975 and 1984. Covariance of the raw PEA time series spanning 1955–97 (35 observations each, using a cubic spline interpolation for gaps) yields correlation coefficients $r = -0.37$, -0.40, and -0.47 for lags of 0, 1, and 2 yr, respectively. These are all significant at the 95% confidence level (for minimum 26, 22, and 16 degrees of freedom, respectively) but are not strong covariance levels. Smoothing improves those covariances to $r = -0.60$ for lags of 0 and 1 yr (significant for 10 or more degrees of freedom). Because different processes dominate each gyre's response to NAO forcing, distinct timescales of response may be expected—for example, one gyre lagging the other. Indeed, it may be more surprising that the two ocean gyres appear to be so closely anticorrelated! From the individual PEA time series we can gain some insights regarding the physical processes, which are the agents of their variability.

b. Subpolar variability

In the Labrador Basin, potential energy is intimately tied to the formation of Labrador Sea Water (LSW): local wind and buoyancy forcing alter the temperature and homogeneity characteristics of the water mass and hence its potential energy. The heat flux anomaly patterns of Cayan (1992b) and Deser et al. (2000) demonstrate a particularly strong connection between the NAO atmospheric SLP patterns and the magnitude of Labrador Basin ocean-to-atmosphere heat fluxes.

A time series of potential temperature at the core of LSW, coplotted in Fig. 5c illustrates its relationship to PEA. In general, the time of persistently low atmospheric NAO (1955–71), when westerlies were weak in the subpolar region, corresponds to a warming LSW and in-

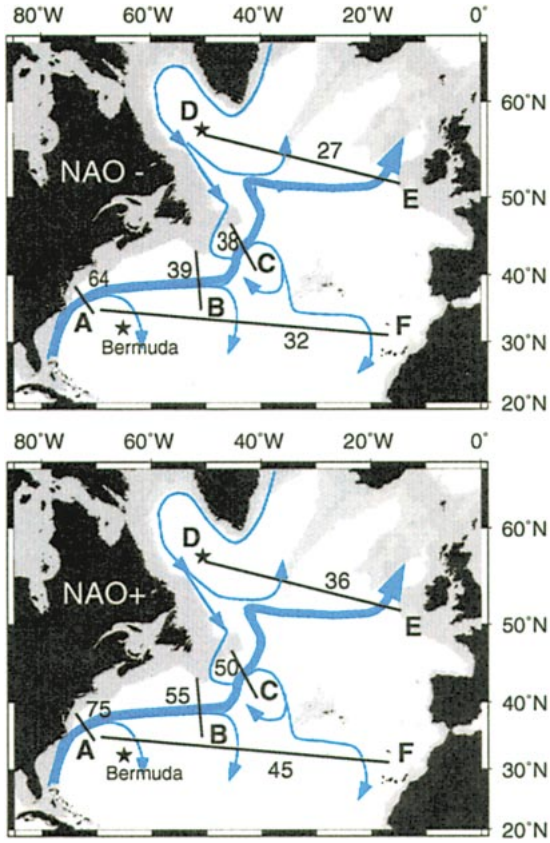

FIG. 12. Schematic representation of the North Atlantic gyre circulation pathways and 0–2000-db baroclinic mass transports in the low NAO (top panel) and high NAO (bottom panel) phases. From the composite maps of PEA distribution in Figs. 4a and 4b, mass transports have been estimated from the PEA difference between locations at the ends of each of five black line segment labeled with the letters **A**–**F**. The transport estimates are the numbers given in units of megatons per second. For example, at position **A**, from the slope water to the peak of the subtropical dome, the transport is estimated as 64 MT s^{-1} in the low NAO phase and 75 MT s^{-1} in the high phase. Line segments **DE** and **AF** in each panel show the net transport for the subpolar and subtropical gyres, respectively.

creasing PEA. Cooling LSW and decreasing PEA are associated with periods of high atmospheric NAO index (1972–76, 1981–84, 1988–95) and strong subpolar westerlies. This time pattern of interannually warming and cooling LSW in the central Labrador Basin, accounting for most of the PEA change, is representative of the western subpolar gyre. Houghton (1996; his Fig. 2, mode M1), for example, has shown similarly structured time series of temperature on pressure surfaces for the Labrador–Newfoundland continental margin.

As will be seen in the discussion of the subtropical gyre below, PEA changes comprise components arising from density changes directly forced by surface buoyancy flux and mixing (diabatic effects), and those due to the main pycnocline moving (quasi-adiabatically) up and down. In the Labrador Sea, convection is typically of order 1000 m (Lazier 1980; Talley and McCartney 1982) but can exceed 2000 m (Clarke and Gascard 1983; Lazier 1995; Lilly et al. 1999). A weak pycnocline separates the LSW from the denser Nordic seas overflow waters but contributes very little through vertical movement to PEA variability. The Labrador Basin 0–2000 db PEA variability predominantly reflects the LSW density history, in turn dominated by the LSW temperature history.

Although freshwater forcing certainly plays a role in the formation of LSW, the PEA changes and overturning transformations are primarily thermally driven phenomena. Over the 40-yr Labrador Basin instrumental record, temperature and salinity, vertically averaged over the upper 2000-db water column, changed by approximately 0.8°C and 0.06 as indicated in Fig. 5d. The relative contributions of these amplitude temperature and salinity changes to density changes determined from the thermal expansion, α, and salinity contraction, β, terms for 3°C and 35.0 psu are: $\alpha\Delta T/\beta\Delta S = -1.55$ at 0 db, -2.00 at 1000 db, and -2.46 at 2000 db. Thus, temperature change had roughly twice the magnitude impact on LSW density compared to salinity change when convection homogenized the surface and deeper layers. The minus sign reflects the opposite sense of density change compared to the subpolar temperature, salinity, and PEA changes. The observed temperature changes drive PEA changes while the observed salinity changes moderate them, opposing the temperature effects but playing the subordinate role. The 0–2000 db PEA history in Fig. 5d tracks closely the vertically averaged temperature, but shows less coordination with the vertically averaged salinity. Moreover, the significant drop in PEA since the 1980s is associated almost exclusively with a temperature decrease of more than 0.6°C. In that same time period, the small net salinity change imparted little effect on density or PEA.

Freshwater forcing in the Labrador Basin reflects a balance of precipitation, evaporation, advection, and vertical mixing. Its history has been colored in particular by occasional, but relatively brief, passages of low salinity surface waters through the region [the ''great salinity anomalies'' (GSAs): Dickson et al. 1988; Belkin et al. 1998], which occupied the Labrador Basin in 1968–72 and again in 1981–84. These are of interest not so much through the direct impact of salinity on LSW density and PEA but rather because the low salinity superficial ''lids'' atop the ocean inhibited convection, thereby blocking the diabatic thermal forcing of deeper density changes. The earlier GSA occupation of the Labrador Basin followed a decadal period of persistently low NAO index during which weak westerlies and negative surface heat flux anomalies had resulted in a gradual curtailing of LSW convection—the LSW steadily growing warmer, more saline, and the central subpolar gyre PEA increasing prior to the GSA buildup in the Labrador Basin (Lazier 1980; Talley and McCartney 1982). The second GSA event, however, coincided with a time of high atmospheric NAO index,

when strong westerlies could have spurred significant convective overturning but did not because of the GSA's interference. This second GSA also followed a couple years of low NAO conditions 1977–79 during which the LSW warmed and PEA increased subsequent to the 1972–76 years of significant cooling and freshening.

During both transits of the Labrador Basin, the GSAs' further inhibition of an already weakened LSW convection confined the ocean–atmosphere heat flux impact to the upper 200–300 m. Below that level warmer, more saline Irminger waters continued to infiltrate the basin, thus leading to increases of PEA. [We note that these events are associated with significant increases in meridional SST gradients of the midlatitude North Atlantic, which may be significant in eliciting an atmospheric response (e.g., Czaja and Marshall 2001)—but that is beyond the scope of this study.] Consecutive winters of cooling eventually caused the surface lid to become dense enough to overturn. Both reinitiations of convection (1972 and 1985) coincided with dramatic alterations of LSW temperature, salinity, and PEA characteristics as the cold fresh lid was convectively mixed into the warmer and more saline LSW that had built up.

Thus, both GSA events in the Labrador Basin coincided with minima in the transport index, while their departures from the Labrador Basin are associated with rapid strengthening of the transport. We reemphasize that PEA changes induced by the reinitiations of convection are dominated by the thermal contributions to density change over the salinity contributions. Although sparse data in the early 1980s prevents determination of many details of the second GSA, it appears that most of the net LSW salinity change ($\Delta S = 0.06$) over the period 1967–94 was incurred by the earlier GSA ($\Delta S = 0.04$). A lingering consequence of the freshening was a shift of PEA (200–400 ergs cm^{-2}) toward higher values than would have otherwise resulted from the 0.7°C LSW temperature decrease alone (~1400 ergs cm^{-2}). The GSAs thus had a slight dampening effect on the intensity of the horizontal circulation post 1972.

Taking into account the GSA occupations in the Labrador Basin, the LSW temperature history resembles the mirror image of the NAO index with one or two years lag. The delay arises from the ocean's sluggish pace of change through time: the LSW does not begin with the same initial conditions each year but instead retains a memory of its state from the previous year. Each year's forcing produces a cumulative effect on the LSW temperature history. Waters exported from the Labrador Basin to the east and south are simultaneously replaced with other waters imported from the east and north, resulting in a slow flushing of the basin (Talley and McCartney 1982). The upstream roots of LSW are found to the east in the deep winter mixed layers, or subpolar mode waters (SPMW: McCartney and Talley 1982), which represent an essential preconditioning (cooling and densification) for the final deep convection that occurs in the Labrador Basin. Alterations of conditions in the SPMW, such as the decadal warming that occurred in the 1960s prior to the GSA and the warming and increased salinity observed along the WOCE A1E/AR7E between 1991 and 1996 (Bersch et al. 1999), therefore must also have an impact on the LSW characteristics downstream. Thus, the subpolar LSW temperature response to NAO forcing primarily involves water mass transformation. Key factors include the intensity of local heat fluxes in the LSW convection area, heat content conditions in the upstream SPMW supply, the residence time of waters in the Labrador Basin, and perhaps changes in the rates of flow in the gyre and overturning circulations. All may be expected to respond to NAO variability through coordinated changes in the air–sea buoyancy flux that directly force progressive convective transformation and through the altered wind strength and patterns that further determine the ocean circulation patterns and intensity.

c. Subtropical gyre variability

In the subtropics, PEA also echoes the upper ocean diabatic thermal history, but other factors are forcing PEA changes; for here the vertical movement of the main pycnocline is significant. In Fig. 5b, analyses of Bermuda temperature anomalies in two layers, 0–500 m and 500–1000 m from Joyce and Robbins (1996), show a strong covariance with the PEA time series. While local and nearby water mass formation can contribute to the 0–500 m temperature history, no nearby water mass formation actively influences the 500–1000 m layer, and diabatic forcing is small, reflecting the main thermocline's mixing intensity (Houghton 1996). Yet even the upper layer does not follow water mass formation history particularly well. The subtropical mode water, or Eighteen Degree Water (EDW), reflecting the local buoyancy forcing, displays a somewhat different history depicted by the time series of EDW temperature from Talley (1996) in Fig. 5a (red curve). The thickness of EDW (or potential vorticity), temperature history, and surface density at Bermuda are significantly correlated to the regional NAO-coordinated buoyancy fluxes (Joyce et al. 2000) but uncorrelated with the depth of the thermocline in the western subtropics and with the temperature near the sea surface (Joyce and Robbins 1996; Houghton 1996). In the surface layer (0–200 m), temperature and salinity are themselves uncorrelated, suggesting that changes in evaporation, precipitation, runoff, or intergyre exchanges may contribute to the surface variability (Talley 1996; Joyce and Robbins 1996; Houghton 1996). In the thermocline layer, temperature, and salinity covary directly through time (Talley 1996; Joyce and Robbins 1996; Houghton 1996), a reflection of the vertical adiabatic displacements of the main pycnocline. Thus, differences between the EDW history and vertically averaged temperature of the 0–500 layer arise from the switching on and off of the local and nearby convective processes, at times se-

questering the EDW from the overlying and underlying strata and at other times producing EDW of different characteristics. Meanwhile basin-scale baroclinic waves are pushing the western basin pycnocline up and down.

Studies of the Bermuda time series indicate that low frequency fluctuations of the western subtropical basin temperature (0–1200 m), steric height, and sea level are all related to shoaling and deepening of the subtropical thermocline (Levitus 1990; Roemmich 1990; Sturges and Hong 1995). This vertical pycnocline displacement in the North Atlantic has been successfully modeled (Sturges and Hong 1995; Sturges et al. 1998; Frankignoul et al. 1997) as a predominantly first baroclinic mode of response to changes in zonally integrated wind stress fields. These studies suggest that, away from the strong circulation regimes of the western boundary, the thermocline depth is primarily wind forced with maximum response in the western basin between longitudes 55°–75°W. Using the actual wind forcing [Comprehensive Ocean-Atmosphere DataSet (COADS)] to hindcast sea level changes, Sturges and Hong (1995) and Sturges et al. (1998) demonstrate a general westward propagation of sea surface height at decadal timescales and reproduce the Bermuda sea level record remarkably well.

An important result of such model studies is that thermosteric sea level changes at Bermuda cannot be solely attributed to either local Ekman pumping or to the zonally averaged wind curl, but instead arise from a zonal integration of the full wind field. This blending of local and remote forcing implies a lag between the atmospheric forcing and the subtropical ocean response that, like the subpolar oceanic response, is not just a simple time delay. In the subtropics, however, the lag reflects not only the local mixed layer and heat flux dynamics but also is related to the phase speed of Rossby waves, the width of the basin, and the ocean's integration of the forcing along those westward propagation pathways. Thus, to the extent that the NAO index captures a significant part of the subtropical gyre-scale wind history, a relation between NAO and baroclinic ocean signals is expected.

d. Thermocline and subthermocline contributions to transport variability

Of the 60 MT s^{-1} mean baroclinic transport defined by the circulation index, more than 90% (56 MT s^{-1} occurs within the depth range of the subtropical gyre's main thermocline, the upper 1000 db. Although less than 5 MT s^{-1} occurs in the deeper depth range, 1000–2000 db, these numbers conceal the geostrophic origins of the upper ocean transport. The Gulf Stream and North Atlantic Current are both linked to deep or bottom reference levels (Fuglister 1963; Worthington 1976; Clarke et al. 1980; Meinen et al. 2000; Sy 1988; Sy et al. 1992). Geostrophic shear in these currents is typically one sign, and thus the transport occurring in the upper 1000 db layer has a component arising from the shear that accumulates from the deep reference level up to the base of that layer. The diagram in Fig. 6g uses the area beneath a profile of dynamic height difference, which is proportional to geostrophic shear, to distinguish between the total mass transported in a layer, the portion of transport due to geostrophic shear in that layer, and the part attributable to the shear in deeper layers. Viewed another way, the 60 MT s^{-1} 0–2000 db baroclinic transport is apportioned as ~47 MT s^{-1} due to shear in the upper 1000 db (compared to ~56 MT s^{-1} amount of referenced transport in that layer), and 13 MT s^{-1} due to the shear between 1000 and 2000 db. Thus, the shear in these deeper layers gives directly ~4 MT s^{-1} transport in that layer but indirectly contributes an additional transport of ~9 MT s^{-1} to the upper 1000 db.

The observed *variability* of the total baroclinic transport can be similarly decomposed into changes in layer transports (i.e., transport in a layer defined by top and bottom pressures, P_1 and P_2, with layer of no motion at P_{ref}, e.g., the stippled horizontal strip in Fig. 6g) and changes of transport due to the shear in a layer (e.g., the vertical hatched strip). From this perspective, a surprising 50% of the 20 MT s^{-1} peak-to-peak transport change derives from alterations of shear beneath the thermocline. Figures 6a–f use three layers: 0–1000 db (thermocline), 1000–1500 db (subthermocline), and 1500–2000 db (deep) to illustrate the time evolution of 1) layer PEA at each gyre center, 2) layer transport referenced to 2000 db (the layer's ''transport index''), and 3) total baroclinic transport (0–2000 db) due to shear in that layer. The net changes of transport in the three layers (0–1000, 1000–1500, 1500–2000) are 17, 2, and 1 MT s^{-1}, respectively; but changes of shear in each layer contribute 9, 6, and 5 MT s^{-1}, respectively, to the total 20 MT s^{-1} change. Thus while variability in observed transports results, as expected, from upper ocean density changes and thermocline displacements, fully half reflects changes in the density field beneath 1000 db. Over the past 25 years, the development of deep geostrophic shear played a significant role in strengthening the total baroclinic transport.

While the 0–2000 db PEA time series (Figs. 3a,b) are approximately equal amplitude mirror images of each other, the gyre PEA changes are maximized in different layers. In the upper 1000 db, changes in the subtropical record (ΔPEA ~ 1000 ergs cm^{-2} dominate those of the subpolar record (ΔPEA ~ 300 ergs cm^{-2}) (Fig. 6a). Thus the 0–1000 db baroclinic layer transport, Fig. 6b (lower curve), echoes the history of the subtropical PEA and is characterized by a long-term decline prior to 1970 followed by a long-term recovery into the 1990s. This nearly symmetrical pattern through time is punctuated by a rapid burst and decline of transport with decadal duration in the 1970s. The transport record between 1975 and 1985 is poorly resolved due to a sparsity of subpolar data so that the details of this shorter duration cycle remain uncertain.

Despite those gaps in the subpolar time series, the

high amplitude and frequency of the 1970s subtropical events are captured not only in the simulated time series by Sturges and Hong (1995) but also in the Bermuda sea level record (Fig. 3d). From this and other modeling studies cited in the preceding section, the subtropical thermocline depth—and here the subtropical 0–1000 db PEA history—are primarily attributable to zonally integrated surface wind stresses. These in turn reflect subdecadal fluctuations of the NAO index in the 1970s. Because the subtropical PEA variability dominates the subpolar variability above 1000 db, the magnitude of vertical shear in the 0–1000 db layer, integrated between the gyre centers—and hence the 0–1000 db baroclinic layer transport—is inferred to be dominated by the heaving of the subtropical thermocline and supplemented by the local buoyancy forcing, for example, the EDW and LSW variability.

A distinctly different behavior characterizes the deepest layer, 1500–2000 db, Figs. 6e and 6f. The shear in this deep layer is rather weak and, with the 2000 db reference level situated at its base, the magnitude of the layer transport is very small ($\sim$1 MT s^{-1}: Fig. 6f). Nonetheless, enough shear accumulates through these 500 db to produce sometimes significant velocities at 1500 db, which then translate into appreciable contributions to the total baroclinic transport. In the first half of the record the deep shear is vanishingly small; but post-1971, shear begins to develop, growing with time so that by the mid-1990s this shear accounts for $\sim$5 MT s^{-1} of the $\sim$20 MT s^{-1} change in total baroclinic transport. It is thus responsible for 25% of the intensified circulation reflected in the transport index during this period.

The middle of the three layers, 1000–1500 db (Figs. 6c and 6d), incorporates aspects of the histories of both the overlying and underlying layers: declining shear before 1972, bursts in the 1970s and 1980s, and development of persistent, enhanced shear in the 1990s. The 1000–1500-db layer transport is weak, varying only from 1 to 3 MT s^{-1} (''Transport Index'': Fig. 6d). It can be characterized as small and nearly constant in the first half of the record, but rising in the second half. The transport due to shear in this layer (Fig. 6d) ranges from 6 to 12 MT s^{-1}, declining in the first half of the record, then not only recovering but with additional growth in the later part of the record. That growth, $\sim$6 MT s^{-1} change in transport due to shear in this layer, represents more than a quarter of the total baroclinic transport gain post-1971.

Viewed as absolute contributions to the total baroclinic transport, there is little that is notable about the deep layers. From the perspective of understanding the evolution of circulation through time, however, the changes in shear of the two deeper layers are significant and surprising. Fluctuations of the subthermocline shear account for fully half of the 20 MT s^{-1} change in 0–2000 total baroclinic transport: that is $\sim$6 and $\sim$5 MT s^{-1} for the two deep layers compared to $\sim$9 MT s^{-1} contributed by shear in the 0–1000 layer.

e. Kinematics and dynamics of secular changes in deep shear

The development of deep shear in the transport index occurs almost exclusively in the last 20 of the 40-yr instrumental record. Prior to 1972, PEA histories for the 1500–2000 db layer are quite similar in both subpolar and subtropical gyres (Fig. 6e) resulting in practically zero shear. Note, however, that PEAs were not constant at the two locations during this period but rather were increasing at the same rate, thus maintaining the small PEA difference between the sites. Changes in the subpolar trend post-1972 contrasted with a continued slow rise of subtropical PEA to produce increased shear, including two bursts in the 1970s and 1980s. Post-1987, the dramatic PEA drop in the subpolar gyre combined with a leveling, and later a slightly declining subtropical PEA, to give rise to a persistent 1500–2000 db layer shear and a significant (4–5 MT s^{-1}) contribution to the total baroclinic transport above 2000 db.

To some degree, the gyre differences in deep PEA evolution stem from distinct responses of the subpolar and subtropical upper deep waters to changes in LSW production. In the subpolar gyre the 1500–2000 db PEA history, like the two shallower layers, largely tracks the LSW formation history (Figs. 5c, 6a, 6c, and 6e) and therefore the local buoyancy forcing modulated by mixed layer dynamics. In the subtropics, interannual changes in this deep layer are formally uncorrelated with those occuring in the thermocline (Roemmich 1990; Joyce and Robbins 1996; Houghton 1996); thus, the subtropical gyre 1500–2000 db PEA history requires a more complex interpretation. The meridional overturning circulation of the North Atlantic flushes the western basin 1500–2000 db layer with the history of LSW characteristics—but not instantaneously. Curry et al. (1998) interpreted this deep layer's interannual temperature history to primarily reflect changes in the volume of LSW exported to the subtropics where it mixes with Mediterranean outflow waters (MOW) to produce Upper North Atlantic Deep Water (UNADW). The timescale of the advective–diffusive mixing of those two water masses and its flushing of the western subtropical gyre introduces a time delay of 5–7 years between the subpolar LSW formation signal and the Bermuda middepth temperature history. The subtropical PEA rises through the first part of the record, but unlike the subpolar record, does not level off for the 1972–88 period: it continues to gently rise until about 1986 and then begins to decline. A few mild reversals (e.g., in 1978 and 1981) are superimposed on the long period of rising PEA, but the observed subtropical PEA history is at best a time-delayed and much muted version of the subpolar gyre PEA history. Superimposed on this advective–diffusive balancing, the main thermocline vertical movements

must also have an impact on the UNADW history through alteration of the background thermal stratification. The interplay between changes in the LSW source endmember and thermocline displacement at times oppose or reinforce each other. The resulting UNADW layer history exhibits characteristics that contain elements of both, enabling divergence of the basin-scale PEA histories and the growth of deep shear.

Such an interpretation of transport fluctuations is largely kinematic: diabatically forced density changes, modulated by adiabatic vertical displacements, interacting through geostrophy to produce transport changes. Modeling studies are needed to replace the diagnosis of geostrophic signatures with higher order dynamics. One element of higher order dynamics is found in the already cited set of model studies in which baroclinic Rossby waves lead to adiabatic displacements of the main thermocline and thus to changes in the regional PEA distribution.

Spall (1996a,b) suggested another dynamical mechanism by which changes in deep density structure could influence a modeled Gulf Stream transport. In this study, the presence of low potential vorticity LSW in the deep western boundary current (DWBC) led to growth and decay of baroclinic instabilities in the deep Gulf Stream, fluctuations in the magnitude of entrainment of waters from the DWBC into the Stream, and enhanced or diminished eastward penetration and circulation depth of the Gulf Stream–North Atlantic Current and their adjacent recirculation cells. These decadal-scale ocean oscillations are self-sustaining in the presence of a constant low potential vorticity LSW in the DWBC and involve growth and decay of deep shear, as in our observations. The study did not explore surface forcing variability or the impacts of a time-varying LSW source on the fluctuating entrainment mechanism. Clearly, several avenues remain for probing the role of ocean dynamics in modulating the gyre circulation intensity.

4. Relation between transport index and atmospheric NAO index

Having examined some individual processes contributing to the interior gyre PEA histories, we next explore the timing of the oceanic transport history relative to forcing correlated with the atmospheric NAO index. As was previously noted, these two signals are not directly covariant. Over the 40-yr instrumental record, the ocean signal appears to slightly lag the atmospheric signal in the sense that the peaks and valleys of the oceanic index occur a year or two later than in the NAO index (Fig. 1). This lag partly reflects the cumulative nature of each ocean gyre's primary responses to atmospheric forcing (e.g., mixed layer temperature content and vertical pycnocline displacement through wave propagation). Additionally, there is advective–diffusive movement of thermal anomalies from one location to another [e.g., SPMW being the upstream source for subpolar LSW, LSW volume and temperature influencing the middepth subtropical water masses, and upper ocean anomalies propagating from subtropics to subpolar regions (as in Sutton and Allen 1997)]. All such processes alter the basin-scale 0–2000 db vertical density structure and give rise to a secondary response: strengthening or weakening of the baroclinic gyre circulation.

In both the subtropical and subpolar gyres, the growth of upper-ocean heat content anomalies involves ocean ''memory''—the ocean does not reset itself each year but instead integrates the forcing through time—whether through diabatic mixed layer/heat flux dynamics or adiabatic baroclinic adjustments of thermocline depth. The integration is not just a local response but blends local and remote forcing influences accumulated along Lagrangian pathways. To formally examine this memory would require a full OGCM simulation with careful consideration of mixed layer physics, wave propagation, and advective pathways; the model studies cited in section 1 are steps in that direction. Other previous work might suggest invoking a first-order Markov autoregressive process to explore the ocean transport response to atmospheric forcing (e.g., Frankignoul and Hasselmann 1977). That model was used, for example, to characterize interdecadal dynamic height variability in the Alaska gyre as a response to stochastic wind forcing through Ekman pumping with linear damping feedback (Lagerloef 1995). However, such a model includes assumptions about the forcing and physics of the response that are not really appropriate to this system. Our transport index involves two gyres for which multiple—and different—physical processes are operating, not solely Ekman pumping. Unlike the wind-driven Alaska gyre, for example, the North Atlantic subpolar gyre variability has significant thermohaline and advective components as well. Moreover, the North Atlantic Ocean dataset is far too limited to estimate the scaling and damping coefficients requisite to a Markov model.

Here we take a simple approach to the observational record with the intention of establishing a basic relationship between the ocean and atmospheric indices: that is, that the transport index reflects fluctuations of the NAO-correlated atmospheric forcing integrated over some timescale(s). Thus, rather than tracking the atmospheric index directly, the ocean response involves a memory of past NAO conditions, but not a prescience of future NAO conditions. We simulate oceanic memory with a low-pass filter of the atmospheric forcing (using the NAO index as a proxy), ''integrating'' backward in time with a built-in decay of influence. We thus replace traditional centered filtering of the NAO index, like the 3-yr running mean of the atmospheric index in Fig. 1 (and repeated in Fig. 7a), with an alternatively filtered version, $A'(t)$, Fig. 7b, in which each point is evaluated as the sum over N previous years weighted decreasingly backward through time by the function Φ:

$$A'(t) = \sum_{n=t}^{t-(N-1)} \frac{\Phi_n A(n)}{\sum \Phi_n},$$

where

$$\Phi_t = 0.42 - 0.5 \cos[2\pi t/(N-1)] + 0.08 \cos[4\pi t/(N-1)].$$

The weighting function is somewhat arbitrary and here implements a one-sided, low-pass filter using a Blackman window. Similar results were produced by other gaussian-type filters, and we conclude that our interpretation is not particularly sensitive to the filter shape. This one was chosen because its behavior in the frequency domain is characterized by a slightly larger central lobe and more rapidly attenuated side lobes—and therefore less sideband leakage—than equivalent length triangular windows. Figure 7d graphs the weighting function in the time domain for four different window widths *N,* indicating that most of its power—or effective memory—is concentrated in the upper 40% of the window. This roughly corresponds to the point where $\Phi_n = 0.5$, while the weights taper rapidly to zero over the remaining width of the window.

As the window width *N* grows from 2 to 10 years, the filtered atmospheric signal quickly begins to resemble the transport index. That similitude is expressed in Fig. 7c by the cross-covariance of the two signals at lags of 0 and 1 yr as a function of *N.* For zero lag, significant correlations ($r > 0.75$, 95% confidence) are associated with integration windows between 6 and 20 years. For *N* between 2 and 13 yr, the correlation is both significant and slightly higher at a 1-yr lag than at zero lag. Indeed, the most satisfactory balance among *r,* significance, and lag arises from an 8–10 yr integration window with 1-yr lag. The filtered index is illustrated in Fig. 7b for several integration windows where the correlation coefficient exceeds 0.75: $N = 8$, 15, 25, and 41. As *N* increases, the amplitude of the filtered signal flattens, but the low frequency characteristics are little changed.

Interpretations of these correlations or lags must be made cautiously considering the short span of the record overlap. Furthermore, sparse subpolar observations between 1975 and 1985 create gaps in the transport index during a critical period where peak-to-peak changes are occurring at 5–6 yr intervals in both signals. Since these peaks and valleys are primarily responsible for the impression of a lagged oceanic response, the data gaps undermine the significance that can be attached to the estimate of lag. No specific timescales for ocean integration can be assessed, nor can a detailed examination of physical linkages be made. Nonetheless, the underlying character of both signals is that of a multidecadal fluctuation, characterized by a steady decrease until 1971 followed by a general increase to 1995, with covarying peaks and valleys of shorter duration. We interpret the behavior of the covariance function to simply reflect the ocean's integration of the atmospheric forcing with one particular expression of that integration being an enhanced or diminished baroclinic gyre circulation. This time slice does suggest that the ocean is at the very least responsive to low frequency fluctuations of the atmospheric forcing, and perhaps even resonant to the decadal and multidecadal components of those fluctuations. Such resonance is manifested in the growth of sometimes large amplitude ocean signals through the integration of a persistent atmospheric phase.

A short-lived impact of the GSAs on the oceanic circulation is also suggested by the brief divergence of the oceanic transport and filtered atmospheric indexes, (Fig. 7b) during the GSA occupations of the Labrador Basin (1968–71 and 1981–84). Both GSA events correspond to minima in the transport index, while their departures from the Labrador Basin are associated with strengthening of the transport index. Note that although the low-salinity surface lids briefly isolate the underlying LSW reservoir from the atmospheric forcing, raising the subpolar PEA and possibly causing the transport index to depart from the filtered atmospheric NAO index, once overturning was reestablished in 1972 and 1985, the transport index converged back with the atmospheric index. The thermal effects of the (NAO-coordinated) atmospheric forcing were temporarily ''stored'' in the surface lid and then subsequently redistributed downward to modify the upper 2000-db density distribution. This emphasizes the thermally driven aspects of the gyre circulation variability, at least for the period spanned by this instrumental record.

5. Comparing the extreme circulation states

A broader geographic context for the PEA time series at Station S and the Labrador Basin can be obtained by compositing hydrographic data for the transport index periods of extreme low (1965–74) and high (1990–97) transport. Figures 4a and 4b map the PEA fields at 200 db relative to 2000 db for the low and high transport time frames. The 200–2000 db values have been used instead of 0–2000 db to limit influences of seasonal heating near the sea surface, although the 0–2000 db maps do not differ too significantly from these except in magnitude. Figure 4c depicts the difference between the two extreme states through color with superimposed contours corresponding to the climatological mean 200–2000 db PEA distribution.

These composites are crude representations of the oceanic state in each of the 8-yr time periods because the sampling is scattered in space and time with abundant gaps in the available hydrographic data (see station locations in Figs. 4d,e). As a result, the composite fields must be used with caution to distinguish mesoscale and seasonal ''noise'' from the signals that reflect the low-frequency changes on which we are focused. Nonetheless, comparing Figs. 4a and 4b suggests that the low frequency fluctuations of PEA described by the Ber-

muda and Labrador Basin time series are representative of basin-scale alterations of the gyres' western interiors.

In the 1990s time of strong transport, the entire subtropical PEA dome west of longitude 40°W was uplifted compared to the earlier weak transport years 1965–74, and the subpolar PEA bowl was deepened. In addition to this north–south dipole, the difference map (Fig. 4c) indicates oppositely signed east–west changes in each gyre for these time frames as well: the eastern subtropics is characterized by a lower (green) PEA while the eastern subpolar region west of Ireland and south of Iceland is higher (yellow colors). This quadripole pattern implies that, when the baroclinic transport index was high (low) circa 1995 (1970), the eastward gyre boundary flows, the southward interior flow of the subtropical gyre, and the northward interior flow of the subpolar gyre were simultaneously strong (weak). However, the timing of these eastern basin anomalies relative to the western basin north–south dipole is not a simple one. They will be explored in somewhat more detail in the following sections.

Small patches of color in the PEA difference map are found in the high gradient regions of the southwest subtropical gyre, Gulf Stream, and North Atlantic Current—mainly the result of eddy structures, lateral shifts, and meandering of these current regimes. Figure 4f maps the standard deviation of the climatological PEA distribution with the mean PEA contours superimposed. To first order, PEA changes along the Gulf Stream–North Atlantic Current should be interpreted as reflecting the meandering of this high gradient band—not necessarily as low frequency changes—since data densities are insufficient to avoid aliasing mesoscale or subannual variability into the current pathway. More moderate variances that characterize broad regions away from the axis of strong flow, however, arise from the decadal changes in heat content and vertical density structure associated with the fluctuations of our transport index. Figure 4c is enlarged in Fig. 8 with six regions identified by boxes labeled **A**–**F**. The changes in each of these regions are explored next.

a. Western subtropics

From 38°–43°N, 55°–65°W, the Gulf Stream and slope water regions are very poorly sampled. In particular, there are only sparse deep profiles in the slope water for the earlier time frame and sparse Gulf Stream crossings in the later period. Because the slope water is fed directly by the deep western boundary current, its subthermocline PEA characteristics (from 1000 to 2000 m) are likely to be similar in amplitude to the Labrador Basin (Talley and McCartney 1982; Pickart et al. 1999). This is true for the 1990s, but little can be actually determined for 1965–74. The PEA difference map shows juxtaposed red and blue patches in the Gulf Stream, which arise from interpolation of very sparse data in a steep gradient, and a high incidence of eddy structures in this area; this region corresponds to the highest rms of PEA (Fig. 4f). Given the spatial gradient and temporal sampling issues, the white circles labeled with red lines in Fig. 8 mark differences that cannot be interpreted as low-frequency variability.

More can be determined about low frequency changes in other regions. The area marked **A** in Fig. 8, situated between 65°–75°W, incorporates the western-intensified peak of the subtropical PEA dome and the region of the Gulf Stream just downstream of its separation from the western boundary. The intensity of PEA difference in this area ($\sim$1000 ergs cm^{-2}) arises from thermocline displacement and from low frequency lateral shifts in the mean Gulf Stream position. Both may be induced by wind forcing and westward propagating planetary waves, although other dynamics may also be involved in this high transport regime of the Gulf Stream and adjacent compact recirculations.

The path of the Gulf Stream in this area has been shown to migrate north–south on various time scales. Seasonal southward displacements of the Stream have been observed to occur in winter to early spring contrasting with northward migrations in the fall (Fuglister 1972; Worthington 1976; Sato and Rossby 1995; Taylor and Stephens 1998; Kelly et al. 1999). Analyses of longer datasets have noted interannual variability of the path that exceeds the seasonal variability (Taylor and Stephens 1998; Joyce et al. 2000). Taylor and Stephens used satellite-based SST and XBT observations to construct an index of mean annual Gulf Stream position (65°–79°W) for the period spanning 1968–98. Joyce et al. (2000) extended the time series back to 1954 basing an alternate index on the intersection of the 15°C isotherm with 200 m depth, determined from BT/XBT measurements between 50° and 75°W. [T. Joyce repeated that analysis using measurements restricted only to the region west of the New England Seamounts (65°–75°W) and is shown here instead of the full longitudinal range of the Gulf Stream.] The details of the two indices vary considerably prior to 1970, yet both show significant covariance with the transport index ($r = 0.74$ and $r = 0.69$, respectively), Fig. 9. This implies a preferentially northern pathway for the Gulf Stream in times of strong transport and a southern pathway when in a weakened state. The sign of PEA composite difference in Fig. 8 is thus quite consistent with path displacements deduced from independent measurements of the Gulf Stream's north wall position.

The two Gulf Stream index studies reached rather different conclusions regarding mechanisms for these observed latitudinal shifts. Taylor and Stephens determined that the position of the north wall lags the NAO index by 2–3 yr, whereas Joyce et al. found a 0–1 yr lag between their index and NAO forcing. However, the version of their index constructed from the western Gulf Stream region, similar to Taylor and Stephens index, is likewise best correlated at a 2-yr lag. Taylor and Stephens invoked arguments similar to those made by Par-

sons (1969), Veronis (1973), and Gangopadhyay et al. (1992), attributing changes in the latitude of the Gulf Stream's separation point from the western boundary and its net geostrophic transport to mass balances of southward Ekman transports integrated across the basin. Gangopadhyay et al. (1992) further speculated that changes in transport of the western boundary current are coupled to the wind stress via westward propagating Rossby waves, as subsequently developed by Sturges and Hong (1995) and Frankignoul et al. (1997). Joyce et al. disagreed that the NAO is forcing a delayed response in Gulf Stream position but instead interpreted a strong correlation at zero lag to indicate the two are varying in phase. They proposed that thermohaline variability in the form of fluctuating subpolar LSW export—as opposed to wind-driving—controls the latitude and timing of Gulf Stream separation and that the zero lag between Gulf Stream position and NAO index could indicate that the latter was responding to the former. We further note that Rossby and Benway (2000) linked time-varying continental shelf transports to north–south shifts of the Gulf Stream and refer the interested reader to these papers for additional details.

These contrasting views perhaps underscore the dangers of attempting to establish causality based on correlations or lags in relatively short time series. To the extent that the Gulf Stream position is strongly coordinated with the fluctuating gyre transport, that the transport variability is delayed relative to the wind forcing history, and that the subtropical PEA history is dominated by vertical thermocline displacements, our analysis suggests that wind forcing and planetary waves play a significant role in the observed Gulf Stream variability. This does not, however, preclude contributions from thermohaline and shelf components. A blending of these components may be responsible for blurring the timescale of oceanic response, or perhaps the dominance of one or more of these mechanisms is variant with time.

Although temporal sampling is sparse, the composite PEA maps of Fig. 4 capture the essence of decadal changes in thermocline depth and Gulf Stream position discussed above. In the 1990s, the average 0–2000 db PEA in Area A seaward of the Gulf Stream reached a value of $\sim$16 000 ergs cm^{-2} compared to only $\sim$15 000 ergs cm^{-2} in 1965–74 when the peak of the dome was also shifted a few degrees offshore and the Gulf Stream separation point and pathway were shifted somewhat to the south. North of the Gulf Stream the slope water region's average PEA (9400 ergs cm^{-2}) did not change appreciably between the two 8-yr time periods. These PEA differences between the 1960s and 1990s are associated with corresponding alterations of the horizontal density gradient—a deepening of the isopycnals on the offshore side of the Gulf Stream, a steepening and shoreward shift of the isopycnals across the current—and reflect an average increase in geostrophic transport from $\sim$64 MT s^{-1} in 1965–74 to $\sim$75 MT s^{-1} in the 1990s.

These alterations of vertical density structure are echoed by PEA changes near Bermuda and further east between longitudes 40°–60°W—the formation region for EDW, the subtropical mode water. Like the peak of the subtropical dome, interdecadal PEA differences in this latter region, marked **B** in Fig. 8, are large ($>$1500 ergs cm^{-2}). The 1990s high PEA values are derived mainly from two hydrographic sections (36°N in 1993 and 52°W in 1997) from which we have removed stations containing cold and warm core rings, easily recognizable on high-resolution synoptic sections. But the XBT dataset, spanning the period 1967–95 with greater time and spatial resolution, confirms the low frequency (quasi-decadal) nature of changes in the region's upper ocean temperatures: the 1990s being more than 1° warmer on average compared to the early 1970s (Fig. 10).

Away from the high gradient region and its lateral shifts, the relative contributions to PEA variability in area **B** can be discerned by comparing vertical profiles of temperature, salinity, density, and PEA from each time frame, as in Fig. 10. Consistent offsets between the time periods are pronounced throughout the upper 1000 m and at LSW depths (1500–2000 m). The amount of interdecadal PEA change for each 100-m interval is shown by the black curve in the bottom right panel of Fig. 10: it is maximal between 800 and 1000 m with smaller peaks near 200 and 1800 m depth. Even here in its formation region, only a small portion of PEA change is attributable to EDW, and hence to regional surface heat flux anomalies. Of the average 1600 ergs cm^{-2} total PEA difference (1990s–60s) accumulated from 2000 db to the sea surface, approximately 300 ergs cm^{-2} is ascribed to warmer, more saline, less dense 1990s EDW (0–500 m); about 1000 ergs cm^{-2} accumulates between 500 and 1200 m because of a deepened thermocline; and about 200 ergs cm^{-2} arises from slightly fresher, less dense waters at LSW levels below 1500 m.

In this region especially, it remains for modeling studies to determine the relative contributions and processes driving these interannual changes. We have already discussed three of these: wind-driven thermocline displacement, local buoyancy flux and EDW water formation, and advective–diffusive movement of subpolar LSW into the deeper strata. But the proximity to the Gulf Stream with its eddy-driven inertial dynamics suggests that other processes may contribute or even dominate. From the composite PEA differences, we posit an eastward extension and elongation of the nonlinear recirculation gyre during the high transport phase and the opposite westward retraction during the low transport period. Model simulations such as those by Spall (1996a,b) and Meacham (2000) exhibit quasi-decadal changes in the penetration depth and lateral extent of the Gulf Stream and its recirculation regime analogous to these observations. The growth and decay of the simulated inertial gyres reflect modes internal to the ocean that are related to the evolution of regional instabilities. Such ocean processes may be competing with or ad-

ditive to the wind and buoyancy forcing in setting the intensity of the gyre transports.

The interdecadal changes in Areas **A** and **B** of the composite maps are consonant with those recorded in the Bermuda time series with slightly greater amplitudes. Vertical profiles of temperature, salinity, density, and PEA at Bermuda (not shown) yield similar, but slightly muted, patterns of offset compared to those for area **B** in Fig. 10. The amount of interdecadal change accumulated in the upper 2000 m at Bermuda is only about 1000 ergs cm^{-2} of which more than 750 ergs cm^{-2} is attributable to thermocline displacement. The contributions to PEA differences from EDW and LSW changes (each ~150 ergs cm^{-2}) are also less pronounced at Bermuda. These amplitude differences may reflect temporal sampling inequities and/or the closer proximity of area **B** to the sources of both EDW and LSW. The essential point is that the Bermuda time series is a respectable indicator of general changes that occurred within the western subtropical gyre from the boundary eastward to about 40°W longitude.

b. Eastern subtropics

The eastern subtropics between 30° and 40°N, 10° and 30°W (area F in Fig. 8) are characterized by interdecadal PEA tendencies opposite to those manifested in the western basin: the 1990s were lower in PEA than the 1960s. These eastern changes are much less a thermocline displacement phenomenon than their western counterparts but instead are mainly attributable to variable influences of MOW near 1000 m depth and LSW between 1500 and 1800 m. The magnitude of area **F** PEA change is 500–700 ergs cm^{-2}, about 50% smaller than in the western basin. The total 700 ergs cm^{-2} change is apportioned as follows: ~150 ergs cm^{-2} between 300 and 800 m depth, ~300 ergs cm^{-2} between 800 and 1400 m, and ~250 ergs cm^{-2} between 1400 and 2000 m.

Vertical profiles of temperature, salinity, density, and PEA near 36°N, 20°W, shown in Fig. 11, illustrate the vertical distribution of properties in each of the extreme transport phases. In the two deeper layers, salinity and temperature exhibit large ranges on depth horizons that are similar for both decadal periods. These ranges reflect regional parcels containing varying intensities of MOW and LSW influences (e.g., Richardson et al. 1991; Paillet et al. 1998). Near 1000 m, the temperature ranges 1.5°C on depth horizons, primarily reflecting the presence of MOW parcels. Below 1500 m in the LSW regime, the temperature range is smaller (~0.5°C) but again similar for both decades. Nearly 80% of the interdecadal PEA signal arises from the strong regional eddy variability at these depths. With the available sampling, these changes cannot be interpreted as low frequency shifts. In the shallower layer (300–800 m), however, the temperature and salinity profiles exhibit a uniform offset between the high and low transport phases, suggesting a slight shoaling of the thermocline in the 1990s relative to the 1965–74 time frame. A similar thermocline shoaling (and subthermocline variability) characterizes the area to the west in the vicinity of the Azores (profiles not shown). Since this reflects local Ekman pumping (Sturges et al. 1998), the phasing of eastern and western basin thermocline displacements depends on the frequency of fluctuations in the wind field. The large PEA change signal in the eastern basin, therefore, is not reflecting a strong mode of ocean variability but instead small thermocline displacements that are overwhelmed by eddy variability in the deeper layers.

c. Mann Eddy–Grand Banks

To the east of Newfoundland and the Grand Banks (area **C**), the north–south PEA dipole elements come directly in contact with one another. Inshore of the Gulf Stream–North Atlantic Current, lower PEA values indicate strong subpolar influences. Offshore, increased PEA values corresponding to the location of the Mann Eddy—a quasi-permanent, anticyclonic circulation feature—signify strong subtropical influences. The mean PEA contours also associate large PEA differences with the steep gradient region, but it is not possible with the available data to determine if this represents a true low frequency shift of the flow axis.

The magnitude of the PEA gradient measured from Flemish Cap to the interior of the Mann Eddy changed substantially between the low and high transport phases: 3800 ergs cm^{-2} during weak transport years compared to 5000 ergs cm^{-2} in the strong phase. The 0–2000 db mass transports associated with these gradients (using f at 45°N) are approximately 38 and 50 MT s^{-1}, respectively. These 1990s enhanced PEA gradients extend northward to about 48°N and eastward out to longitude 40°W, but the additional transport then appears to be recirculated to the south between longitudes 35° and 45°W; the higher subtropical PEA contour values do not continue northeastward but instead turn southward just to the west of the Azores. It demonstrates that one manifestation of the enhanced circulation state is an eastward extension of the subtropical gyre as in model studies by Spall (1996a,b) and Meacham (2000), but it also suggests that this does not necessarily result in a simultaneous net increase of northward transport into the subpolar regions. Poor sampling in both time frames, however, precludes any robust conclusions with the available observations.

d. Subpolar gyre

A stronger 1990s subpolar circulation is manifested by lowered PEA in the west (area **D**, Fig. 8) opposing increased PEA values in the east (area **E**); while in the weak transport phase, opposite conditions prevailed. The 8-yr PEA composites (Figs. 4a and 4b) depict an east–west PEA gradient of magnitude 3000 ergs cm^{-2}

for the weak phase, with an associated baroclinic mass transport of ~27 MT s^{-1} (using f at 50°N), compared to 4000 ergs cm^{-2} and ~36 MT s^{-1} in the time of strong transport. This gyre intensification is further reflected in enhanced 1990s trans-Atlantic spreading rates of LSW documented through its time varying temperature/salinity and chlorofluorocarbon signatures (Cunningham and Haine 1995a,b; Sy et al. 1997; Cunningham 2000).

Interdecadal PEA changes in the western basin, (Fig. 8, area **D**) were discussed in section 3b; the peak-to-peak change (1971 vs 1993) is approximately 1000 ergs cm^{-2} but the average difference determined between the two 8-yr time periods (1965–74 vs 1990–97) is only about 500 ergs cm^{-2}, as depicted in the composite difference map. Like the western subpolar basin, the development of PEA anomalies in the eastern basin partly reflects local buoyancy forcing. But other physical mechanisms also contribute in proportionally large ways: advective–diffusive movement of intermediate water masses such as LSW (e.g., Cunningham and Haine 1995a,b), upper-ocean thermal anomalies through the reemergence mechanism (Alexander and Deser 1995), and wind-driven alterations of the subpolar front (e.g., Lorbacher 2000; Esselborn and Eden 2001, manuscript submitted to *J. Climate*, hereafter EE). Because these mechanisms generate different response times, the phasing of eastern subpolar PEA anomalies with respect to the western basin is neither a simple nor stationary relationship.

Several years (4–5) are required for advective–diffusive movement of middepth water masses from the Labrador Basin to the eastern basin (e.g., Cunningham and Haine 1995a,b; Sy et al. 1997). This spreading rate appears to vary with time and has been linked to NAO fluctuations in LSW production (Sy et al. 1997; Koltermann et al. 1999). Likewise, there is a delay for upper-ocean heat content anomalies to propagate from the west (e.g., Reverdin et al. 1997; Sutton and Allen 1997) and for heat content anomalies to develop locally through air–sea heat flux. In contrast, oceanic heat transport across 48°N is quite responsive to NAO shifts in the wind stress curl incurring little or no delay relative to the forcing (Lorbacher 2000; EE). In the eastern subpolar basin, a post-1996 PEA rise of order 500 ergs cm^{-2} (yellow–orange colors) reflected a significant warming and density decrease in the deep winter mixed layers, or SPMW, following the dramatic drop of the NAO index in winter 1995/96 (Bersch et al. 1999). This warming was also captured in the altimeter data as a basinwide thermosteric rise in sea-surface height of order +8 cm and attributed mainly to shifts of wind stress curl (EE) resulting in increased lateral heat transport, which was supplemented by locally decreased surface heat fluxes (Bersch et al. 1999; Reverdin et al. 1999). Opposite cold, fresh upper ocean conditions rapidly infiltrated the same region following the 1972 shift in NAO from extended low to a high phase. The cold, fresh properties were rooted in advective–diffusive mixing of anomalous waters originating from the Labrador Current (Reverdin et al. 1997). As the Gulf Stream–NAC was at that time in a very weakened state, the anomaly of circulation strength may also have contributed to those eastern basin alterations by building anomalously cool, fresh conditions in the western subtropics of the late 1960s.

While both eastern and western subpolar PEA variability are delayed relative to NAO forcing through mixed layer dynamics and advective–diffusive import of water properties, the eastern basin is additionally subject to substantial and rapid changes of its PEA characteristics induced by NAO shifts in the wind stress curl. The lateral transport of oceanic heat and salt across 48°N is enhanced in low NAO and diminished under wind stress patterns associated with the high NAO phase (Koltermann et al. 1999; Lorbacher 2000). This in turn contributes to a complicated east–west phasing of subpolar PEA and a baroclinic circulation that is at times enhanced (as in the 1990s) and at other times weak (1966–74).

e. Cross-basin transport estimates

Although crude, the composite PEA maps reinforce the sense of changes in gyre circulation intensity suggested by the Bermuda–Labrador Basin transport index. Figure 12 summarizes the differences between the extreme NAO phases using transport estimates derived from PEA gradients at several key locations annotated along the Gulf Stream–North Atlantic Current. A progressional decrease of transports in the downstream direction reflects the divergence of the boundary current flow. Strictly speaking, therefore, the transport index does not measure directly the eastward baroclinic flow (which weakens from west to east) but rather is proportional to the magnitude of combined flows in both gyres. A more accurate measure of the gyre transports could be obtained with additional time series measurements in the eastern basins and slope water regions. For example, in the composite diagrams of Fig. 12 the lines connecting points **D**–**E** and **A**–**F** give the cross-basin PEA difference and hence the strength of each gyre's meridional transports. The subtropical and subpolar gyre transports respectively are thus estimated to be 32 and 27 (total 59) MT s^{-1} in the weak transport phase and 45 and 36 (total 81) MT s^{-1}, in the 1990s. The average transport index for these same 8-yr periods are 52 and 65 MT s^{-1} for the weak and strong phases, respectively. Because the Bermuda endmember does not measure the peak of the subtropical dome, the transport index attains only 82%–88% of the totals estimated from the maximum east–west gradients. However, as the bulk of PEA changes occur in the western basin, it is fair to assert that the transport index captures the essence and pace of low-frequency baroclinic changes occurring in the gyre circulations.

6. Summary and conclusions

Our analysis of 0–2000 db PEA history from the instrumental record documents a significant (>30%) fluctuation in a portion of the North Atlantic gyre circulation over the past 50 years. A two-point baroclinic pressure difference between the subpolar and subtropical gyre centers provides the basis for a transport index—an oceanic analogue to the widely used SLP-based atmospheric NAO indices. It describes an interdecadal cycle of weakening followed by a progressional strengthening of the eastward baroclinic flow in the upper 2000 db from its 48 MT s^{-1} minimum circa 1970 to a maximum state exceeding 65 MT s^{-1} in the 1990s. That strengthening involved a surprising amplitude symmetry of the subpolar and subtropical gyres, each gyre's 0–2000 db PEA varying by ~1000 ergs cm^{-2} between the extremes. To some degree, the gyre PEA histories are fluctuating in antiphase. That phase relationship is a tentative one, however, reflecting latitudinal shifts of the surface westerlies across the North Atlantic but also reflecting differences in the forcing mechanisms and responses that contribute to each gyre's PEA history.

Changes in vertical density structure of the central subpolar gyre are primarily thermally driven but punctuated by the occasional passages of low-salinity GSAs through the region. The PEA history reflects a combination of factors: 1) buoyancy forcing acting locally to produce convective overturning—and remotely to alter conditions upstream in the SPMW, 2) flushing of the Labrador Basin with waters imported from the north and east, and 3) low-salinity surface caps advected into the region that briefly inhibit convective overturning and ultimately impart a freshening to the depth of subsequent convective penetration. The subpolar gyre may be expected, therefore, to respond not only to NAO-coordinated changes in air–sea buoyancy fluxes and Ekman forcing but also to changes in the ocean's baroclinic circulation strength. In the western basin particularly, the ocean response is sluggish, reflecting an accumulation of the atmospheric forcing through mixed layer dynamics and variability in the rates at which waters are imported and exported from the interior basin.

The subtropical response to NAO variability is also a blend of local and remote forcing. The PEA fluctuations of the western interior gyre are dominated by vertical displacements of the main pycnocline and supplemented by changes in the locally formed EDW and by changes in deep density structure related to advective–diffusive import of LSW. Other dynamics, related to the strong inertial recirculation regime of the Gulf Stream, may be important as well: the inertial gyre's PEA signature exhibits an eastward extension and westward retraction associated with the strong and weak transport phases, respectively. The EDW records the history of local air–sea buoyancy fluxes, and its contribution to the subtropical PEA variability is significant but considerably smaller than changes incurred by vertical displacements of the main pycnocline. Shoaling and deepening of the pycnocline in the gyre center are primarily a response to zonally integrated wind stresses through westward propagating planetary waves. At the phase speeds associated with the first baroclinic mode, these waves require several years to cross the width of the Atlantic and exhibit maximum amplitudes in the western basin (Sturges and Hong 1995; Frankignoul et al. 1997; Sturges et al. 1998). The impact of LSW variability on the subtropical middepths is likewise delayed (5–7 yr) relative to the subpolar source region by the timescales of advective–diffusive processes (Curry et al. 1998; Koltermann et al. 1999) and potentially through self-sustaining decadal oscillations of deep Gulf Stream energetics related to the LSW's low potential vorticity (Spall 1996a,b). It is uncorrelated with the thermocline fluctuations, but the development of deep shear plays a significant role in boosting the baroclinic transport, accounting for fully half of the 20 MT s^{-1} change in 0–2000 db total transport over the instrumental record. Thus, to the extent that the NAO index captures a significant part of the subtropical basin-scale wind history, a relation between NAO and subtropical baroclinic signals is expected. A lag in the ocean response reflects not only the local mixed layer, surface flux dynamics but also the ocean's integration of the atmospheric forcing across the width of the basin and the growth and decay of shear in the subthermocline layers related to NAO-coordinated changes in LSW overturning.

The Labrador Basin and Bermuda time series are representative of vertical density structure changes manifested broadly throughout the western basins. Composites of the PEA distributions at the extremes of the transport index not only confirm the basinwide geographic scale of the quasi-decadal north–south dipole but also indicate east–west changes occurring on these timescales. The resulting pattern of interdecadal PEA difference translates to increased meridional as well as zonal baroclinic transports, and thus significantly stronger horizontal circulations in both subpolar and subtropical gyres of the 1990s compared to 25 years before. That is, when the baroclinic transport index was high (low) circa 1995 (1970), the eastward gyre boundary flows, the southward interior flow of the subtropical gyre, and the northward interior flow of the subpolar gyre were simultaneously strong (weak).

Although an east–west seesaw character of subtropical PEA change is suggested in the Sturges et al. (1998) dynamic height patterns and westward propating baroclinic waves, that phasing is a tentative characterization and subject to future monitoring and sorting out its underlying mechanisms. The contribution of thermocline displacement to eastern subtropical PEA variability (~150 ergs cm^{-2}) is far smaller than in the western basin (750–1000 ergs cm^{-2}). Eddy variability from regionally distributed parcels of MOW and LSW overwhelms the PEA information in the eastern basin's

sparse hydrographic record creating a false expression of a large signal.

By contrast, interdecadal changes in the eastern subpolar PEA (~500 ergs cm^{-2}) and dynamic height are large and reflect a variety of mechanisms and time scales of response. NAO shifts in wind stress curl drive particularly large and rapid changes in heat transport in the vicinity of the gyre boundary. Interannual modulations of water mass transformation in the deep winter mixed layers of the SPMW, fluctuations of overturning strength in the Labrador Basin, and advection of upper ocean thermal anomalies originating in the subtropics and Labrador Current have also contributed significantly to the eastern basin PEA history.

The strength of gyre flows at the extreme transport phases was estimated from PEA gradients at several locations along the gyre boundary and from the east–west cross-basin PEA differences. These estimates reinforce the sense of changes in gyre circulation intensity reflected in the Bermuda–Labrador Basin transport index. From Cape Hatteras at the western boundary to Ireland in the east, a progressional decrease of transport reflects the divergence of the boundary current flow. The transport index, therefore, does not directly measure the eastward baroclinic flow (which weakens from west to east) but rather is proportional to the magnitude of combined flows in both gyres. Because the Bermuda endmember does not measure the peak of the subtropical dome, the transport index attains only ~85% of the total transport magnitude estimated from the maximum east–west gradients. Nonetheless, the transport index captures the essence and pace of low frequency variability exhibited in the gyre circulations.

This analysis underscores the need to move beyond passive-response, mixed layer representations of the ocean in assessing climate variability. It suggests a system that grows sometimes large signals through the interaction of several factors: diabatic mixed layer/air–sea flux anomalies; planetary waves; intergyre exchanges of heat, salt, and mass in the thermocline and deeper layers; and perhaps baroclinic instabilities in the deep Gulf Stream system. At times these factors are additive (e.g., at the extremes of the transport index) and at other times opposing (between the transport extremes). The resultant weakened or strengthened gyre circulation can thus be more—or less—efficient at transporting heat, salt, and other climatically relevant properties from one location to another. Anomalies of circulation strength may therefore play an important role in building heat anomalies as well as moving them geographically beneath the overlying atmosphere.

The timescales on which the gyre intensifies and weakens are dependent partly upon the frequencies of the atmospheric forcing (e.g., surface heat fluxes, wind stress patterns) but also directed in part by factors internal to the ocean's dynamics (e.g., phase speed of planetary waves, advective–diffusive processes, growth and decay of deep Gulf Stream instabilities). As demonstrated by the model simulation of SST by Halliwell (1998), on seasonal to interannual timescales, surface turbulent heat fluxes dominate the open-ocean temperature response but on decadal–interdecadal scales, anomalies of circulation are important. Simulation and prediction of climate variability will therefore require fully coupled models that reproduce the ocean's baroclinic adjustment as well as mixed layer dynamics. The transport index presented here is one benchmark against which models may be compared to observed ocean variability.

Acknowledgments. The authors thank Bob Molinari for contributing his time series of XBT data. We also thank Terry Joyce and Arnold Taylor who lent us their time series of Gulf Stream positions. Bob Dickson and an anonymous reviewer provided helpful comments for which we are most appreciative. This research was supported by NOAA Award NA76GP0348 and NSF Grants OCE-9617946 and OCE-9529606.

REFERENCES

Alexander, M. A., and C. Deser, 1995: A mechanism for the recurrence of wintertime midlatitude SST anomalies. *J. Phys. Oceanogr.,* **25,** 122–137.

Barnston, A. G., and R. E. Livezey, 1987: Classification, seasonality and persistence of low-frequency atmospheric circulation patterns. *Mon. Wea. Rev.,* **115,** 1083–1126.

Battisti, D. S., U. S. Bhatt, and M. A. Alexander, 1995: A modeling study of the interannual variability in the wintertime North Atlantic Ocean. *J. Climate,* **8,** 3067–3083.

Belkin, I. M., S. Levitus, J. I. Antonov, and S.-A. Malmberg, 1998: ''Great Salinity Anomalies'' in the North Atlantic. *Progress in Oceanography,* Vol. 41, Pergamon, 1–68.

Bersch, M., J. Meincke, and A. Sy, 1999: Interannual thermocline changes in the northern North Atlantic 1991–1996. *Deep-Sea Res. II,* **46,** 55–75.

Bjerknes, J., 1964: Atlantic air–sea interaction. *Advances in Geophysics,* Vol. 10, Academic Press, 1–82.

Bunker, A. F., 1976: Computations of surface energy flux and annual air–sea interaction cycles of the North Atlantic Ocean. *Mon. Wea. Rev.,* **104,** 1122–1140.

Capotondi, A., and W. R. Holland, 1997: Decadal variability in an idealized ocean model and its sensitivity to surface boundary conditions. *J. Phys. Oceanogr.,* **27,** 1072–1093.

Cayan, D. R., 1992a: Latent and sensible heat flux anomalies over the northern oceans: Driving the sea surface temperature. *J. Phys. Oceanogr.,* **22,** 859–881.

——, 1992b: Latent and sensible heat flux anomalies over the northern oceans: The connection to monthly atmospheric circulation. *J. Climate,* **5,** 354–369.

Clarke, R. A., and J.-C. Gascard, 1983: The formation of Labrador Sea Water. Part 1: Large-scale processes. *J. Phys. Oceanogr.,* **13,** 1764–1778.

——, H. W. Hill, R. F. Reiniger, and B. A. Warren, 1980: Current system south and east of the Grand Banks of Newfoundland. *J. Phys. Oceanogr.,* **10,** 25–65.

Cunningham, S. A., 2000: Circulation and volume flux of the North Atlantic using synoptic hydrographic data in a Bernoulli inverse. *J. Mar. Res.,* **58,** 1–35.

——, and T. W. N. Haine, 1995a: Labrador Sea Water in the eastern North Atlantic. Part I: A synoptic circulation inferred from a minimum in potential vorticity. *J. Phys. Oceanogr.,* **25,** 649–665.

——, and ——, 1995b: Labrador Sea Water in the eastern North Atlantic. Part II: Mixing dynamics and the advective–diffusive balance. *J. Phys. Oceanogr.,* **25,** 666–678.
Curry, R. G., 1996: HydroBase: A database of hydrographic stations and tools for climatologic analysis. Woods Hole Oceanographic Institution Tech. Rep. 96-01, 50 pp.
——, M. S. McCartney, and T. M. Joyce, 1998: Oceanic transport of subpolar climate signals to mid-depth subtropical waters. *Nature,* **391,** 575–577.
Czaja, A., and J. Marshall, 2001: Observations of atmospheric–ocean coupling in the North Atlantic. *Quart. J. Roy. Meteor. Soc.,* in press.
Delworth, T., 1996: North Atlantic interannual variability in a coupled ocean–atmosphere model. *J. Climate,* **9,** 2356–2375.
——, S. Manabe, and R. J. Stouffer, 1993: Interdecadal variations of the thermohaline circulation in a coupled ocean–atmosphere model. *J. Climate,* **6,** 1993–2011.
Deser, C., 2000: On the teleconnectivity of the ''Arctic Oscillation.'' *Geophys. Res. Lett.,* **27,** 779–782.
——, and M. L. Blackmon, 1993: Surface climate variations over the North Atlantic Ocean during winter: 1900–1989. *J. Climate,* **6,** 1743–1753.
——, J. E. Walsh, and M. S. Timlin, 2000: Arctic sea ice variability in the context of recent atmospheric circulation trends. *J. Climate,* **13,** 617–633.
Dickson, R. R., J. Meincke, S. A. Malmberg, and A. J. Lee, 1988: The great salt anomaly in the northern North Atlantic 1968–1982. *Progress in Oceanography,* Vol. 20, Pergamon, 103–151.
——, J. Lazier, J. Meinke, P. Rhines, and J. Swift, 1996: Long-term coordinated changes in the convective activity of the North Atlantic. *Progress in Oceanography,* Vol. 38, Pergamon, 241–295.
Esselborn, S., and C. Eden, 2001: Sea surface height changes in the North Atlantic Ocean related to the North Atlantic Oscillation. *J. Climate,* submitted.
Ezer, T., 1999: Decadal variabilities of the upper layers of the subtropical North Atlantic: An ocean model study. *J. Phys. Oceanogr.,* **29,** 3111–3124.
Fofonoff, N. P., 1962: Dynamics of ocean currents. *The Sea: Ideas and Observations on Progress in the Study of the Seas.* Vol. 1: *Physical Oceanography,* M. N. Hill, Ed., John Wiley and Sons, 323–395.
——, and R. C. Millard, 1983: Algorithms for computation of fundamental properties of seawater. Unesco Technical Papers in Marine Science 44, 53 pp.
Frankignoul, C., and K. Hasselmann, 1977: Stochastic climate models: Part II. Application to sea surface temperature anomalies and thermocline variability. *Tellus,* **29,** 289–305.
——, P. Müller, and E. Zorita, 1997: A simple model of the decadal response of the ocean to stocastic wind forcing. *J. Phys. Oceanogr.,* **27,** 1533–1546.
Fuglister, F. C., 1963: Gulf Stream '60. *Progress in Oceanography,* Vol. 1, Pergamon, 265–373.
——, 1972: Cyclonic rings formed by the Gulf Stream 1965–66. *Studies in Physical Oceanography—A Tribute to Georg Wüst on His 80th Birthday,* A. L. Gordon, Ed., Vol. 1, Gordon and Breach, 137–168.
Gangopadhyay, A., P. Cornillon, and R. D. Watts, 1992: A test of the Parsons–Veronis hypothesis on the separation of the Gulf Stream. *J. Phys. Oceanogr.,* **22,** 1286–1301.
Greatbatch, R. J., and J. Xu, 1993: On the transport of volume and heat through sections across the North Atlantic: Climatology and the pentads 1955–1959, and 1970–1974. *J. Geophys. Res.,* **98,** 10 125–10 143.
——, A. F. Fanning, A. G. Goulding, and S. Levitus, 1991: A diagnosis of interpentadal circulation changes in the North Atlantic. *J. Geophys. Res.,* **96,** 22 009–22 023.
Griffies, S. M., and K. Bryan, 1997: A predictability study of simulated North Atlantic multidecadal variability. *Climate Dyn.,* **13,** 459–487.
Grötzner, A., M. Latif, and T. P. Barnett, 1998: A decadal climate cycle in the North Atlantic Ocean as simulated by the ECHO coupled GCM. *J. Climate,* **11,** 831–847.
Häkkinen, S., 1999: Variability of the simulated meridional heat transport in the North Atlantic for the period 1951–1993. *J. Geophys. Res.,* **104,** 10 991–11 007.
——, 2000: Decadal air–sea interaction in the North Atlantic based on observations and modeling results. *J. Climate,* **13,** 1195–1219.
Halliwell, G. R., 1997: Decadal and multidecadal North Atlantic SST anomalies driven by standing and propagating atmospheric anomalies. *J. Climate,* **10,** 2405–2411.
——, 1998: Simulation of North Atlantic decadal/multidecadal winter SST anomalies driven by basin-scale atmospheric circulation anomalies. *J. Phys. Oceanogr.,* **28,** 5–21.
Hansen, D. V., and H. F. Bezdek, 1996: On the nature of decadal anomalies in North Atlantic sea surface temperature. *J. Geophys. Res.,* **101,** 9749–9758.
Hasselmann, K., 1976: Stochastic climate models: Part I. Theory. *Tellus,* **28,** 473–485.
Houghton, R. W., 1996: Subsurface quasi-decadal fluctuations in the North Atlantic. *J. Climate,* **9,** 1363–1373.
Hurrell, J. W., 1995: Decadal trends in the North Atlantic Oscillation regional temperatures and precipitation. *Science,* **269,** 676–679.
——, 1996: Influence of variations in extratropical wintertime teleconnections on Northern Hemisphere temperature. *Geophys. Res. Lett.,* **23,** 665–668.
——, and H. van Loon, 1997: Decadal variations in climate associated with the North Atlantic oscillation. *Climatic Change,* **36,** 301–326.
Jones, P. D., T. Johnson, and D. Wheeler, 1997: Extension to the North Atlantic oscillation using early instrumental pressure observations from Gibraltar and south–west Iceland. *Int. J. Climatol.,* **17,** 1433–1450.
Joyce, T. M., and P. E. Robbins, 1996: The long-term hydrographic record at Bermuda. *J. Climate,* **9,** 3121–3131.
——, C. Deser, and M. A. Spall, 2000: On the relation between decadal variability of subtropical mode water and the North Atlantic oscillation. *J. Climate,* **13,** 2550–2569.
Kelly, K. A., S. Singh, and R. X. Huang, 1999: Seasonal variations of sea surface height in the Gulf Stream region. *J. Phys. Oceanogr.,* **29,** 313–327.
Koltermann, K. P., A. V. Sokov, V. P. Tereschenkov, S. A. Dobroliubov, K. Lorbacher, and A. Sy, 1999: Decadal changes in the thermohaline circulation of the North Atlantic. *Deep-Sea Res.,* **46,** 109–138.
Kushnir, Y., 1994: Interdecadal variations in North Atlantic sea surface temperature and associated atmospheric conditions. *J. Climate,* **7,** 141–157.
Lagerloef, G. S. E., 1995: Interdecadal variations in the Alaska gyre. *J. Phys. Oceanogr.,* **25,** 2242–2258.
Lazier, J. R. N., 1980: Oceanographic conditions at Ocean Weather Ship BRAVO, 1964–1974. *Atmos.–Ocean,* **18,** 227–238.
——, 1995: The salinity decrease in the Labrador Sea over the past thirty years. *Climate on Decade-to-Century Time Scales,* National Academy of Sciences Press, 295–302.
Leetmaa, A., and A. F. Bunker, 1978: Updated charts of the mean annual wind stress, covergences in the Ekman layers and Sverdrup transports in the North Atlantic. *J. Mar. Res.,* **36,** 311–322.
Levitus, S., 1989a: Correction to ''Interpentadal variability of temperature and salinity at intermediate depths of the North Atlantic Ocean, 1970–1974 versus 1955–1959'' by Sydney Levitus. *J. Geophys. Res.,* **94,** 14 599.
——, 1989b: Interpentadal variability of temperature and salinity at intermediate depths of the North Atlantic Ocean, 1970–1974 versus 1955–1959. *J. Geophys. Res.,* **94,** 6091–6131.
——, 1990: Interpentadal variability of steric sea level and geopotential thickness of the North Atlantic Ocean, 1970–1974 versus 1955–1959. *J. Geophys. Res.,* **95,** 5233–5238.
Lilly, J. M., P. B. Rhines, M. Visbeck, R. Davis, J. R. N. Lazier, F. Schott, and D. Farmer, 1999: Observing deep convection in the

Labrador Sea during winter 1994/95. *J. Phys. Oceanogr.,* **29,** 2065–2098.

Lorbacher, K., 2000: Niederfrequente Variabilitaet meridionaler Transporte in der Diver-genzzone des nordatlantischen Subtropen- und Subpolarwirbels—Der WOCE-Schnitt A2. Berichte des Bundesamt für Seeschi Hahrt und Hydrographie No. 22, 156 pp.

Lozier, M. S., W. B. Owens, and R. G. Curry, 1995: The climatology of the North Atlantic. *Progress in Oceanography,* Vol. 36, Pergamon, 1–44.

Mazoguchi, K., S. D. Meyers, S. Basu, and J. J. O'Brien, 1999: Multi- and quasi-decadal variations of sea surface temperature in the North Atlantic. *J. Phys. Oceanogr.,* **29,** 3133–3149.

McCartney, M. S., and L. D. Talley, 1982: The subpolar mode water of the North Atlantic Ocean. *J. Phys. Oceanogr.,* **12,** 1169–1188.

Meacham, S. P., 2000: Low-frequency variability in the wind-driven circulation. *J. Phys. Oceanogr.,* **30,** 269–293.

Meinen, C. S., D. R. Watts, and R. A. Clarke, 2000: Absolutely referenced geostrophic velocity and transport on a section across the North Atlantic current. *Deep-Sea Res.,* **47,** 309–322.

Molinari, R. L., D. Mayer, J. Festa, and H. Bezdek, 1997: Multi-year variability in the near surface temperature structure of the mid-latitude western North Atlantic Ocean. *J. Geophys. Res.,* **102,** 3267–3278.

Paillet, J., M. Arhan, and M. S. McCartney, 1998: Spreading of Labrador Sea Water in the eastern North Atlantic. *J. Geophys. Res.,* **103,** 10 223–10 239.

Parsons, A. T., 1969: Two layer model of Gulf Stream separation. *J. Fluid Mech.,* **39,** 511–528.

Pickart, R. S., T. K. McKee, D. J. Torres, and S. A. Harrington, 1999: Mean structure and interannual variability of the slopewater system south of Newfoundland. *J. Phys. Oceanogr.,* **29,** 2541–2558.

Reverdin, G., D. Cayan, and Y. Kushnir, 1997: Decadal variability of hydrography in the upper northern North Atlantic in 1948–1990. *J. Geophys. Res.,* **102,** 8505–8531.

——, N. Verbrugge, and H. Valdimarsson, 1999: Upper ocean variability between Iceland and Newfoundland 1993–1998. *J. Geophys. Res.,* **104,** 29 599–29 611.

Richardson, P. L., M. S. McCartney, and C. Maillard, 1991: A search for meddies in historical data. *Dyn. Atmos. Oceans,* **15,** 241–265.

Roemmich, D., 1990: Sea level and the thermal variability of the ocean. *Sea Level Change, Studies in Geophysics,* National Research Council, National Academy Press, 208–217.

Rogers, J. C., 1990: Patterns of low-frequency monthly sea level pressure variability (1899–1986) and associated wave cyclone frequencies. *J. Climate,* **3,** 1364–1379.

——, 1997: North Atlantic storm track variability and its association to the North Atlantic Oscillation and climate variability of northern Europe. *J. Climate,* **10,** 1635–1647.

Rossby, T., and R. L. Benway, 2000: Slow variations in mean path of the Gulf Stream east of Cape Hatteras. *Geophys. Res. Lett.,* **27,** 117–120.

Saravanan, R., and J. C. McWilliams, 1997: Stocasticity and spatial resonance in interdecadal climate fluctuations. *J. Climate,* **10,** 2299–2320.

——, and ——, 1998: Advective ocean–atmosphere interaction: An analytical stocastic model with implications for decadal variability. *J. Climate,* **11,** 165–188.

——, G. Danabasogli, S. C. Doney, and J. C. McWilliams, 2000: Decadal variability and predictability in the midlatitude ocean–atmosphere system. *J. Climate,* **13,** 1073–1097.

Sato, O., and T. Rossby, 1995: Seasonal and low frequency variations in dynamic height anomaly and transport of the Gulf Stream. *Deep-Sea Res.,* **42,** 149–164.

Spall, M. A., 1996a: Dynamics of the Gulf Stream/deep western boundary current crossover. Part I: Entrainment and recirculation. *J. Phys. Oceanogr.,* **26,** 2152–2168.

——, 1996b: Dynamics of the Gulf Stream/deep western boundary crossover. Part II: Low-frequency internal oscillations. *J. Phys. Oceanogr.,* **26,** 2169–2182.

Sturges, W., and B. G. Hong, 1995: Wind forcing of the Atlantic thermocline along 32°N at low frequencies. *J. Phys. Oceanogr.,* **25,** 1706–1715.

——, ——, and A. J. Clarke, 1998: Decadal wind forcing of the North Atlantic subtropical gyre. *J. Phys. Oceanogr.,* **28,** 659–668.

Sutton, R. T., and M. R. Allen, 1997: Decadal predictability in Gulf Stream sea surface temperatures. *Nature,* **399,** 563–565.

Sy, A., 1988: Investigation of large-scale circulation patterns in the central North Atlantic: The North Atlantic Current, the Azores Current, and the Mediterranean Water plume in the area of the Mid-Atlantic Ridge. *Deep-Sea Res.,* **35,** 383–413.

——, U. Schauer, and J. Meincke, 1992: The North Atlantic Current and its associated hydrographic structures above and eastwards of the Mid-Atlantic Ridge. *Deep-Sea Res.,* **39,** 825–853.

——, M. Rhein, J. R. N. Lazier, K.-P. Koltermann, J. Meincke, A. Putzka, and M. Bersch, 1997: Surprisingly rapid preading of newly formed intermediate waters across the North Atlantic Ocean. *Nature,* **386,** 675–679.

Talley, L. D., 1996: North Atlantic circulation and variability reviewed for the CNLS conference. *Physica D,* **98,** 625–646.

——, and M. S. McCartney, 1982: Distribution and circulation of Labrador Sea Water. *J. Phys. Oceanogr.,* **12,** 1189–1205.

Taylor, A. H., and J. A. Stephens, 1998: The North Atlantic Oscillation and the latitude of the Gulf Stream. *Tellus,* **50A,** 134–142.

van Loon, H., and J. C. Rogers, 1978: The seesaw in winter temperatures between Greenland and Northern Europe. Part I: General description. *Mon. Wea. Rev.,* **106,** 296–310.

Veronis, G., 1973: Model of world ocean circulation: I. Wind-driven, two-layer. *J. Mar. Res.,* **31,** 228–288.

Visbeck, M., H. Cullen, G. Krahmann, and N. Naik, 1998: An ocean model's response to North Atlantic Oscillation—like wind forcing. *Geophys. Res. Lett.,* **25,** 4521–4524.

Worthington, L. V., 1976: *On the North Atlantic Circulation.* Johns Hopkins Oceanographic Studies, No. 6, 110 pp.

Wunsch, C., 1999: The interpretation of short climate records with comments on the North Atlantic and Southern Oscillations. *Bull. Amer. Meteor. Soc.,* **80,** 245–256.